eLife

Reviewed Preprint
v1 • April 28, 2026
Not revised

For correspondence:
wenjun.xiong@cityu.edu.hk

Competing interests: W.X. and B.L. are inventors on a pending patent application (Priority No. 18/820,216) related to the CCA vector used in this study. All other authors declare no competing interests.

Funding: See page 41

Reviewing editor: Xiaorong Liu, University of Virginia, United States

Synergistic Inhibition of Notch Signaling and Forced Cell Cycle Re-entry Drive Müller Glia Reprogramming in Uninjured Mouse Retina

Baoshan Liao[1], Chengshang Lyu[1], Yuqing Jiang[1], Shanggong Liu[1], Waiho Wong[1], Jiadong Zhang[3,4], Hoyin Tsang[1], Junxi Xie[1], Lingxi Chen[1], Qinrong Zhang[3], Wenjun Xiong[1,2]

[1]Department of Biomedical Sciences, College of Biomedicine, City University of Hong Kong, Hong Kong, China • [2]Key Laboratory of Biochip Technology, Biotech and Health Centre, Shenzhen Research Institute of City University of Hong Kong, Shenzhen, China • [3]Department of Biomedical Engineering, College of Biomedicine, City University of Hong Kong, Hong Kong, China • [4]Hong Kong Centre for Cerebro-Cardiovascular Health Engineering (COCHE), Hong Kong, China

eLife Assessment

This study shows that combining forced cell cycle re-entry with Rbpj deletion enhances Müller glia dedifferentiation and promotes their conversion into retinal neuron-like cells in the uninjured mouse retina. It provides a **valuable** strategy for improving Müller glia-mediated neurogenesis and advancing regenerative potential in the mammalian retina. Overall, the data are **convincing**, but the conclusions would be strengthened by functional validation of the newly generated neurons and retinal performance, as well as an assessment of Müller glia long-term function and cell survival.

https://doi.org/10.7554/eLife.111251.1.sa2

Abstract

In regenerative species, such as teleost fish, Müller glia (MG) autonomously re-enter the cell cycle after injury and give rise to functional retinal neurons. In contrast, the loss of retinal neurons in mammals is irreversible due to the limited proliferative and regenerative ability of MG. Various strategies have been developed to induce proliferation of mature mouse MG with or without injury, yet most MG daughter cells retain glial cell fate. Here, we found that MG progenies maintain high Notch signaling, which may constrain their neurogenic potential. Conditional deletion of *Rbpj*, the central transcriptional effector of Notch, induced limited MG-to-neuron conversion in mature MG without proliferation. However, *Rbpj* deletion, combined with forced MG proliferation by overexpressing cyclin D1 and suppressing $p27^{Kip1}$, significantly promoted MG dedifferentiation and ectopic expression of the neuronal marker Otx2 in MG daughter cells in uninjured mouse retina. Combining Notch inhibition with MG cell cycle re-activation not only increased the numbers of bipolar- and amacrine-like cells generated from MG but also promoted the further differentiation toward ON-cone, OFF-cone, and rod-bipolar subtypes. Single-nucleus RNA and ATAC sequencing data revealed that Notch inhibition facilitated the formation of MG-derived progenitor-like cells while MG proliferation increased chromatin accessibility of neurogenic genes. Notably, most MG-derived cells survived long term despite incomplete maturation. Together, our findings delineate how Notch inhibition and MG proliferation, alone or in combination, influence the regenerative potential of MG in the mammalian retina.

Introduction

Müller glia share a common lineage with retinal neurons, serving as the only glial cell type differentiated from retinal progenitor cells (RPCs) while retaining a transcriptomic profile similar to their progenitors(1–3). Beyond their role in maintaining retinal homeostasis, MG function as a latent stem cell population in lower vertebrates. In zebrafish, retinal injury triggers a robust regenerative response wherein quiescent MG dedifferentiate, re-enter the cell cycle, and undergo asymmetric division to self-renew and generate multipotent retinal progenitors. These progenitor cells subsequently differentiate to regenerate all major retinal neuron types, replacing damaged cells(4–6). However, this regenerative capacity is progressively restricted across vertebrate evolution. While MG in young chicks can initiate a single mitotic cycle and transition to MG-derived progenitor cells (MGPCs), MGPCs only differentiate into amacrine cells and bipolar cells(7, 8). In mice and humans, MG lack the intrinsic capacity to autonomously re-enter the cell cycle or regenerate lost neurons, representing a major barrier to treating retinal degenerative diseases(2, 6, 9).

Overcoming MG quiescence is the first step toward regeneration. We previously demonstrated that the high level of $p27^{Kip1}$, a cell cycle inhibitor, and the low level of cyclin D1 in mature mouse MG prevent them from re-entering the cell cycle. Concurrent downregulation of $p27^{Kip1}$ and upregulation of cyclin D1, which was delivered via a single AAV vector termed the Cell Cycle Activator (CCA), synergistically promote MG proliferation. CCA-driven MG proliferation further promoted the dedifferentiation of MG following mitosis, but the vast majority of MG eventually reverted to their glial identity(10). Similarly, direct activation of the Wnt/β-catenin signaling pathway or bypassing the Hippo pathway via overexpressing Hippo non-responsive form of YAP (YAP5SA) also led to spontaneous re-entry into the cell cycle and transiently reprogramming into a progenitor cell-like state, but no regeneration of mature neurons was reported(11–13). These findings indicate that while cell proliferation is necessary to expand the MG pool and initiate dedifferentiation, it is insufficient to drive functional neurogenesis, implying that the existence of additional molecular barriers that enforce glial identity.

Notch signaling represents a primary candidate for this barrier. During development, Notch acts as a binary switch, maintaining the RPC pool and specifying glial fate. Downregulation of Notch is required for neuronal differentiation, whereas sustained activity promotes MG formation(12, 14, 15). After development, this pathway remains active in mature MG, enforcing quiescence in the uninjured retina(14, 16). In zebrafish, injury induces the downregulation of Notch receptors and downstream target genes *Hes*/*Hey* family, thereby derepressing the proneural genes *Ascl1* to promote neurogenesis(6, 14, 17–19). Conversely, in mammalian central nervous system, Notch signaling actively suppresses neurogenesis in contexts ranging from the cortex to the cochlea(20–23). Recent studies in the mouse retina have shown that disrupting Notch, particularly in combination with knockout of *Nuclear factor I a/b/x* (*Nfi a/b/x*) or overexpressing the Yamanaka factor, *octamer-binding transcription factor 4* (*Oct4*), enhance MG reprogramming efficiency(24, 25).

In this study, we investigated why postmitotic MG fail to yield neurons. We found that Notch signaling remains active in the postmitotic MG-derived cells, which may prevent their diversion toward a neuronal fate. We hypothesized that inhibition of Notch signaling would unlock the neurogenic potential of proliferating MG. By combining CCA treatment with MG-specific deletion of the Notch transcriptional effector, *Recombination signal binding protein for immunoglobulin kappa J region* (*Rbpj*), we achieved robust reprogramming of MG into bipolar- and amacrine-like neurons in uninjured adult mouse retina. Single-nucleus RNA sequencing (snRNA-seq) and RNA *in situ* hybridization revealed that these newborn neurons exhibit a retinal neuron transcriptional signature, expressing markers characteristic of amacrine cells and subtypes of bipolar cells. Single nucleus ATAC-sequencing (snATAC-seq) analysis demonstrated that CCA treatment induced chromatin opening at key neurogenic genes, a priming event that is functionally capitalized upon by Notch inhibition. Notably, the reprogrammed MG displayed long-term survival up to 9 months

post-treatment. Together, our study demonstrated the synergistic effects of cell proliferation and Notch inhibition on MG reprogramming in the absence of retinal injury, providing molecular and temporal insights into this process.

Results

CCA-induced MG progeny maintains high Notch signaling

In our previous study, we developed an AAV vector CCA that overexpresses cyclin D1 and knock down $p27^{Kip1}$ (Fig. 1a)(10). When injected intravitreally to uninjured adult mouse eyes, CCA potently stimulated nearly half of the MG to proliferate (Fig. 1a-c, Fig. S1a-c). This CCA-driven proliferation is highly efficient, yet remains self-limiting, with MG typically undergoing a single cell division(10). The kinetics of CCA-induced MG proliferation are age-dependent. In neonatal pups, CCA triggers MG to enter the cell cycle faster, whereas in postnatal day 28 (P28) mice, MG proliferation starts later and is a more prolonged process, typically occurring between 1 and 4 weeks after CCA injection (Fig S1b). Following mitosis, these MG transiently and partially dedifferentiated, downregulating glial gene *Glul* and *Sox9* while upregulating progenitor marker *Gadd45a/b/g*(10). However, by four months post-treatment, the vast majority of postmitotic MG revert to their original glial identify (Fig. 1b-c). Fewer than 1% MG completely lost MG identity, as shown by negative Sox9 staining (Fig. 1c), while expressing high levels of Otx2, a pro-neuronal marker (Fig. 1d).

To understand this blockade in neurogenesis, we analyzed the single-cell RNA sequencing (scRNA-seq) data from our previous study(10) to characterize the activity of Notch signaling in postmitotic MG. We found that key Notch signaling components, including the receptor *Notch1*, the central regulator *Rbpj*, and the downstream effector *Hes1*, remained highly expressed in postmitotic MG following cell cycle re-activation (Fig S1d-g). In contrast, these genes were expressed at negligible levels in native retinal neurons, such as rod photoreceptors (Fig S1f-g).

We confirmed this finding using RNA *in situ* hybridization for *Hes1*. In control retinas, *Hes1* mRNA was abundant in MG within the inner nuclear layer (INL) but minimal in the photoreceptors residing in the outer nuclear layer (ONL) (Fig. 1e-f). In CCA-treated retinas, even MG-derived cells had migrated to the ONL, high *Hes1* mRNA levels maintained comparable to quiescent MG (Fig. 1e-f). Given the established role of Notch as a suppressor of neurogenesis, we hypothesized that this persistent activity constitutes the primary barrier preventing CCA-treated MG from differentiating into neurons.

Rbpj deletion in late RPC promotes rod genesis at the expense of MG and bipolar cells

To validate our genetic approach of Notch inhibition in MG, we utilized *Glast-*Cre^{ERT2}*;*$Rbpj^{flox/flox}$*;tdT* or *Sun1:GFP* mice. *Rbpj* is the obligate nuclear mediator all Notch receptors, and its deletion abolishes canonical Notch signaling(26–28). We first confirmed that tamoxifen (TAM)-induced deletion of *Rbpj* in adult mice resulted in the complete loss of *Hes1* mRNA (Fig. S2a-e).

Glast is a marker gene expressed in RPCs in neonatal mice and later restricted to the specified MG(29, 30). To examine the effects of *Rbpj* loss on cell fate determination of the late RPCs, we induced *Rbpj* deletion in the late RPCs at P1 and analysed the retinas at P12 (Fig. S3a-b). *Rbpj*-/- retinas had a significantly higher proportion of late-born rod photoreceptors compared to the control and *Rbpj*+/- retinas, with no effect on the early-born cone photoreceptors (Fig. S3c-d, Fig. S4a-c). Conversely, *Rbpj* deletion significantly impaired the generation of MG (Sox9+) and bipolar cells (Otx2+ in the INL) from late RPCs (Fig. S3c, e, Fig. S5a-c).

The generation of amacrine cells and retinal ganglion cells (RGCs) remained unaffected (Fig. S6a-c, Fig. S7a-c). These developmental data confirm that *Rbpj* removal biases progenitors toward a photoreceptor at the expense of MG and bipolar cells, consistent with the previous report using *Notch1* knockout in the late PRCs(31).

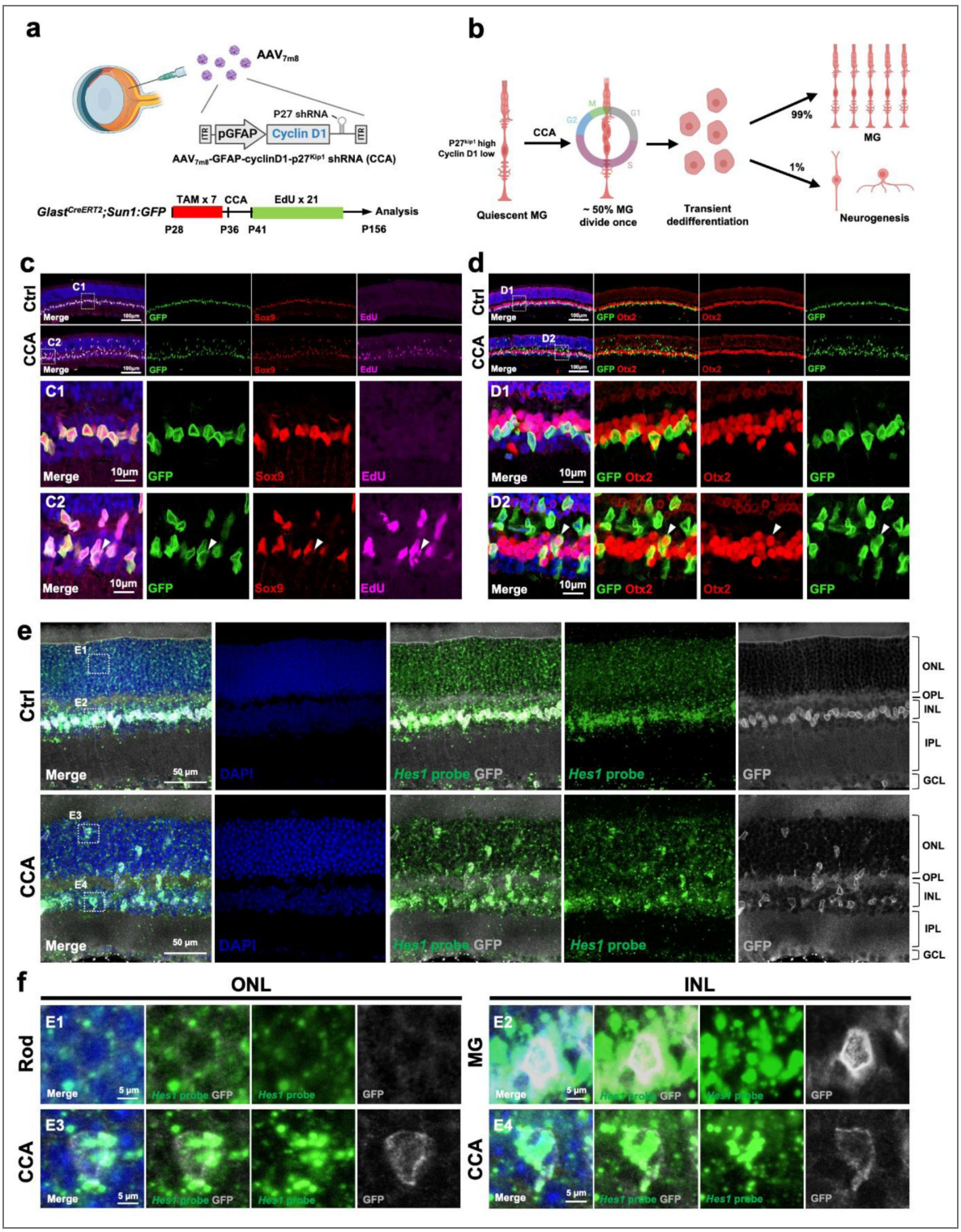

Figure 1. MG and MG-derived cells maintained high level of Notch signaling.

(a) Schematic representations of the intravitreal injection of AAV_{7m8}-GFAP-cyclinD1-$p27^{Kip1}$ shRNA-WPRE (CCA). (b) The overview process of MG proliferation induced by CCA. (c) Representative Sox9 and EdU immunostaining on retinal sections from *Glast-Cre^{ERT2};Sun1:GFP* mice treated with CCA at P28 and collected 4 months post-treatment. C1-C2 are the magnified views of the highlighted regions. The white arrows refer to GFP+ EdU+ Sox9- cells. (d) Representative Otx2 immunostaining on retinal sections from *Glast-Cre^{ERT2};Sun1:GFP* mice treated with CCA at P28 and collected 4 months post-treatment. D1-D2 are the magnified views of the highlighted regions. The white arrows refer to GFP+ Otx2+ cells. (e) Hes1 mRNA *in situ* hybridization in the control and the *Glast-Cre^{ERT2};Sun1:GFP* mouse retinas harvested at four months post CCA injection. (f) Magnified views of the highlighted regions in (e). n=3 mice.

Rbpj loss in mature MG triggers inefficient direct glia-to-neuron conversion

We next tested whether Notch inhibition alone is sufficient to reprogram mature MG. We induced *Rbpj* deletion in fully developed retinas at P28 and analysed them at 3 weeks and 4 months post-treatment (Fig. 2a). At 3 weeks, all *Rbpj* KO MG expressed the glial marker Sox9 (Fig. 2b–d). However, by 4 months, approximately 7.6% of GFP-positive MG-derived cells had lost Sox9 and 7.5% had begun expressing the neuronal marker Otx2 (Fig. 2e, Fig. S8a-c). These findings indicate that Notch inhibition alone elicits a slow, progressive dedifferentiation in a subset of MG over time. Unlike in the developmental context, no photoreceptor-like cells were formed. Of note, these *Rbpj*-deficient MG did not incorporate EdU (Fig. S9a–b), indicating that Notch inhibition unlocks a slow, inefficient transdifferentiation process without inducing cell cycle activation.

Notch inhibition reduces but does not abolish CCA-induced MG proliferation

Since direct conversion depletes MG, we aimed to combine CCA-induced proliferation to expand the MG pool with *Rbpj* KO-driven reprogramming. Because Notch inactivation drives premature cell-cycle exit during development(31–33), we first determined if *Rbpj* deletion would antagonize the mitogenic activity of CCA. We administrated TAM from P28 to P35 to induce *Rbpj* KO, followed by CCA injection at P36 (Fig. S10a). Subsequently, EdU was administrated intraperitoneally daily for 21 days, spanning the major time window of MG proliferation, and the mice were then harvested afterwards to assess MG proliferation (Fig. S10a). Notch inhibition reduced MG proliferation induced by CCA, but it did not completely halt the process, as the number of EdU+ MG was reduced in *Rbpj*-/- mice compared to the wild type and *Rbpj*+/- controls (Fig. S10b-c). Reversing the orders of TAM and CCA treatments yielded similar results (Fig. S10d-g). These data indicate that while Notch inhibition exerts an anti-proliferative effect, overexpression of cyclin D1 and suppression of $p27^{Kip1}$ are sufficient to override this blockade and maintain a robust proliferative response, consistent with the fact that cyclin D1 and $p27^{Kip1}$ are downstream of Notch signaling(34).

Combining *Rbpj* deletion and CCA treatment induce robust MG dedifferentiation and ectopic expression of Otx2

We next evaluated the reprogramming efficiency of the combined treatment of CCA and *Rbpj* KO. Ideally, *Rbpj* deletion should be induced immediately after MG proliferation. However, CCA-driven MG proliferation is a prolonged, asynchronized process. To ensure precise lineage tracing and minimize confounding effects of CCA on gene expression, we adopted the protocol of administrating TAM immediately prior to CCA injection (Fig. S11a). At 3 weeks post-treatment, MG in all groups retained Sox9 expression (Fig. S11b-d). By 4 months, approximately 27.8% of GFP-positive MG-derived cells in the combination group had lost Sox9 expression, a significantly higher fraction than in the CCA alone (1.5%) or *Rbpj* KO alone (7.6%) groups (Fig. S11b-e). Importantly, the total number of Sox9+ MG remained higher in the combination group than that in the control, indicating that the combined treatment did not deplete the glial pool (Fig. S11f).

The enhanced dedifferentiation was accompanied by more robust neurogenesis. At 3 weeks, lineage tracing revealed no Otx2+ MG-derived cells in the combination group (Fig. 3a-d). At 4 months, about 27.4% of tdT+ MG expressed Otx2 in the combined treatment group, significantly higher than that of the CCA-only group (Fig. 3b-e, Fig. S12a). Compared to *Rbpj* deletion alone, Otx2+ MG percentage was increased by three folds in the combined treatment (Fig. 3e).

Given that photoreceptor loss is a leading cause of incurable blindness worldwide(35, 36), reprogramming MG into photoreceptors represents a promising therapeutic strategy. We examined whether MG-derived cells adopted photoreceptor identities. In the combination group, a subset of postmitotic MG in the ONL upregulated photoreceptor markers, including Otx2 (12.8% of ONL td+ EdU+ MG) and Crx (8.2% of ONL tdT+ EdU+ MG), consistent with potential progression

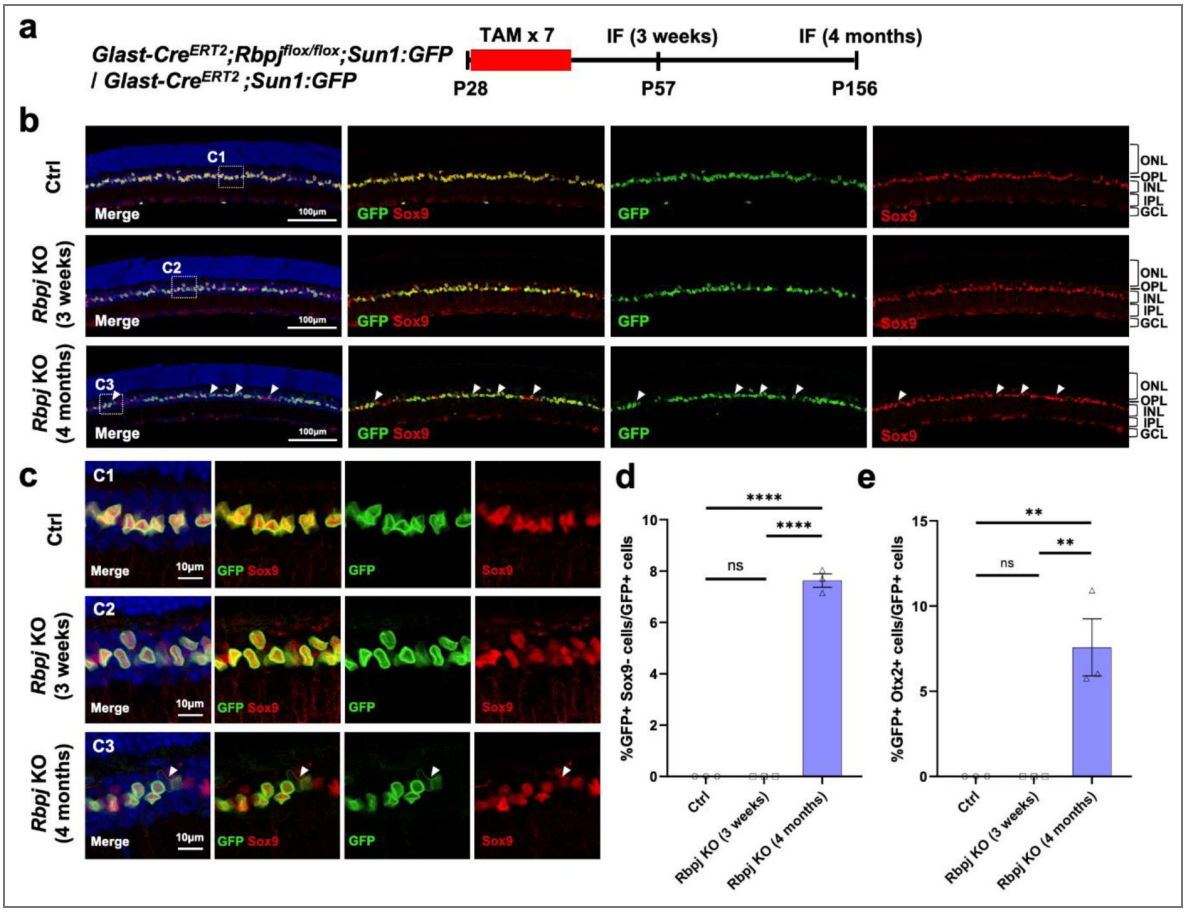

Figure 2. ***Rbpj*** **deletion in adult MG induces limited dedifferentiation**

(a) Schematic illustration of MG dedifferentiation and reprogramming experiment. (b) Representative immunostaining of Sox9 on retinal sections from *Glast-Cre^{ERT2};Sun1:GFP* and *Glast-Cre^{ERT2};Rbpj$^{flox/flox}$;Sun1:GFP* mice in different timepoints post TAM injection. The white arrows refer to GFP+ Sox9- cells. (c) Magnified views of the highlighted regions in (b). (d) Percentage of GFP+ Sox9- cells in overall GFP+ cells. n=3 mice, data are presented as mean ± SEM. ns=not significant, ****$P < 0.0001$, by one-way ANOVA with Tukey's post hoc test. (e) Percentage of GFP+ Otx2+ cells in overall GFP+ cells. n=3 mice, data are presented as mean ± SEM. ns=not significant, **$P < 0.01$, by one-way ANOVA with Tukey's post hoc test.

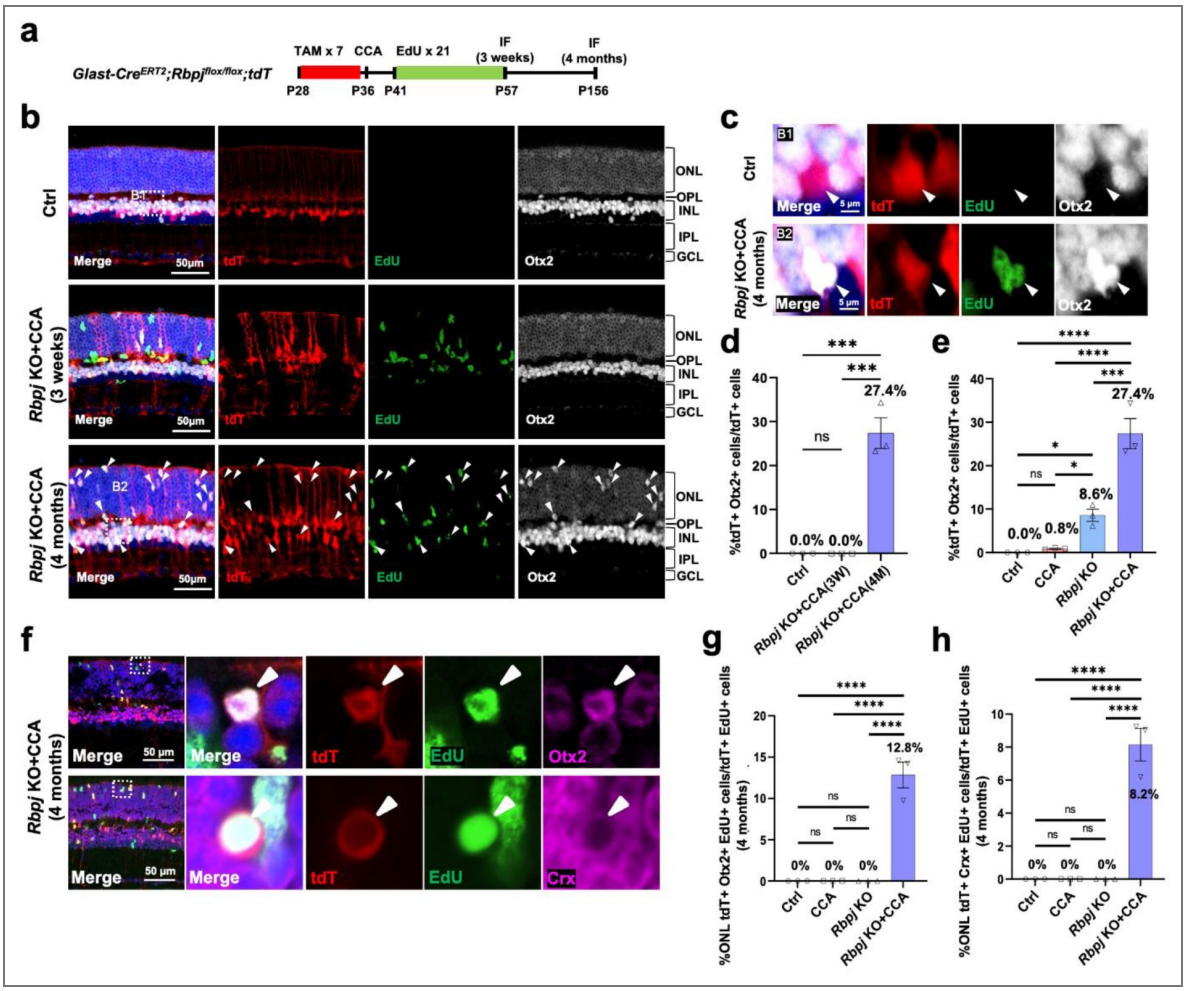

Figure 3. ***Rbpj*** **KO and CCA synergistically increase Otx2+ cell formation from MG**

(a) Schematic illustration of the neurogenesis assessment experiment. (b) Representative immunostaining of EdU and Otx2 on retinal sections. The white arrows refer to tdT+ Otx2+ cells. (c) Magnified views of the highlighted regions in (b). The white arrows refer to tdT+ Otx2+ cells. (d) Percentage of tdT+ Otx2+ cells in overall tdT+ cells. 3W: 3 weeks, 4M: 4 months, n=3 mice, data are presented as mean ± SEM. ns=not significant, ***$P < 0.001$, by one-way ANOVA with Tukey's post hoc test. (e) Percentage of tdT+ Otx2+ cells in overall tdT+ cells. n=3 mice, data are presented as mean ± SEM. ns=not significant, *$P < 0.05$, ***$P < 0.001$, ****$P < 0.0001$, by one-way ANOVA with Tukey's post hoc test. (f) Representative immunostaining of EdU and Otx2 or Crx on retinal sections. (g) Percentage of tdT+ EdU+ Otx2+ cells in ONL tdT+ EdU+ cells. n=3 mice, data are presented as mean ± SEM. ns=not significant, ****$P < 0.0001$, by one-way ANOVA with Tukey's post hoc test. (h) Percentage of tdT+ EdU+ Crx+ cells in ONL tdT+ EdU+ cells. n=3 mice, data are presented as mean ± SEM. ns=not significant, ****$P < 0.0001$, by one-way ANOVA with Tukey's post hoc test.

toward photoreceptor fate (Fig. 3f–h). The soma of some MG-derived cells in the ONL also adopted a photoreceptor cell-like circular morphology but without any structure of outer segment (Fig. 3f). However, only about 2% of ONL MG-derived cells expressed *Nrl*, an important factor regulating the rod photoreceptor specification(37) (Fig. S12b-c), which may limit maturation into fully developed rod photoreceptors.

In summary, these findings collectively demonstrate that the combined treatment of CCA and *Rbpj* deletion significantly enhances both the dedifferentiation of MG and the subsequent generation of retinal neurons compared to either treatment alone.

Rbpj deletion promotes the formation of neuronal progenitor cells from MG

To dissect the transcriptional trajectory of reprogramming, we performed snRNA-seq on purified MG from *Glast-Cre^{ERT2};Rbpj$^{flox/flox}$;Sun1:GFP* mice (Fig. 4a). We analyzed four experimental groups, the untreated control (Ctrl), CCA treatment (CCA), *Rbpj* deletion (*Rbpj* KO), and combined *Rbpj* deletion and CCA treatment (*Rbpj* KO+CCA), at 1 week, 3 weeks, and 4 months post-treatment (Fig. 4a).

No significant batch effects were observed across the treatment groups (Fig. S13a). Following quality control filtering and the exclusion of native mature neurons, which were uniformly distributed across all three timepoints and treatment groups, approximately 3,500 to 12,000 cells were remained for downstream snRNA sequencing analysis (Fig. S13a-b). The uniform manifold approximation and projection (UMAP) visualization of snRNA-seq data revealed dynamic cell cluster transitions over time (Fig. 4b-c). Clustering analysis identified eight MG-related populations: quiescent MG, reactivated MG, proliferating MG, MGPCs, transitional MG, amacrine cell (AC)-like MG and bipolar cell (BC)-like MG, annotated using known retinal markers (Fig. 4b–d, Fig. S13c-d, Fig. S14a-b).

At 1 week, prior to peak transgene expression, MG in the control and *Rbpj* KO groups remained quiescent, expressing high levels of MG genes (*Aqp4*, *Rlbp1*, *Kcnj10*) (Fig. 4b–d, Fig. S14a–c, Fig. S15a). In contrast, CCA treatment drove cells into a “reactivated” state marked by upregulation of the gliosis genes (*Gfap*, *Vim*), likely a response to AAV infection (Fig. 4b–d, Fig. S14a–c, Fig. S15a). At this time, no proliferating cells were observed in the CCA-injected eyes, as the AAV-mediated transgene expression had not reached the level required to drive the cell cycle.

At 3 weeks, the divergence between treatments became evident. In the CCA treated groups, MG (6.4% in CCA and 2.2% in *Rbpj* KO+CCA) proliferated (Fig. S14c). A subset of MG in *Rbpj* KO (3.4%) and *Rbpj* KO+CCA (4.0%) upregulated neurogenic factors (*Neurog2*, *Ascl1*, *Dll1*), marking them as MGPCs (Fig. 4b–d, Fig. S14a–c, Fig. S15a). A small fraction (<1%) of nascent AC-like cells (expressing *Elavl3*, *Rbfox3*, *Caln1*) and BC-like cells (expressing *Gsg1*, *Pcdh17*, *Lgr5*) emerged in *Rbpj* KO MG at this stage (Fig. 4b–d, Fig. S14a–c, Fig. S15a). By 4 months, while CCA-only MG had largely reverted to quiescence with minimal neurogenesis, the *Rbpj* KO and *Rbpj* KO+CCA groups sustained high percentages of MGPCs (21.5% and 23.5%, respectively) (Fig. 4b–d, Fig.S14b–c, Fig. S15a), confirming that Notch inhibition drives MGPC formation. Neurogenesis progressed significantly by this stage, with the combined treatment yielding a higher percentage of AC-like cells (*Rbpj* KO, 3.2%; *Rbpj* KO+CCA, 2.2%) and BC-like cells (*Rbpj* KO, 9.9%; *Rbpj* KO+CCA, 18.3%) compared to the CCA-only group (Fig. 4b–d, Fig. S14b–c, Fig. S15a), Additionally, a unique “transitional” cluster enriched for mitochondrial gene (*mt-Cytb*, *mt-Nd4*) appeared in the *Rbpj* KO+CCA group (Fig. 4b–d, Fig. S14b–c, Fig. S15a), suggesting a metabolically active state conducive to reprogramming.

To elucidate the mechanism by which *Rbpj* deficiency promotes neurogenic potential, we performed differential gene expression analysis on 3-week reactivated MG, a critical inflection point between quiescence and commitment to MGPC. At this time point, the CCA-treated reactivated MG cluster exhibited heightened expression of genes associated with quiescent MG (*Hes5*, *Lgals9*) (Fig. 4e). The elevated expression levels of genes linked to quiescent MG may

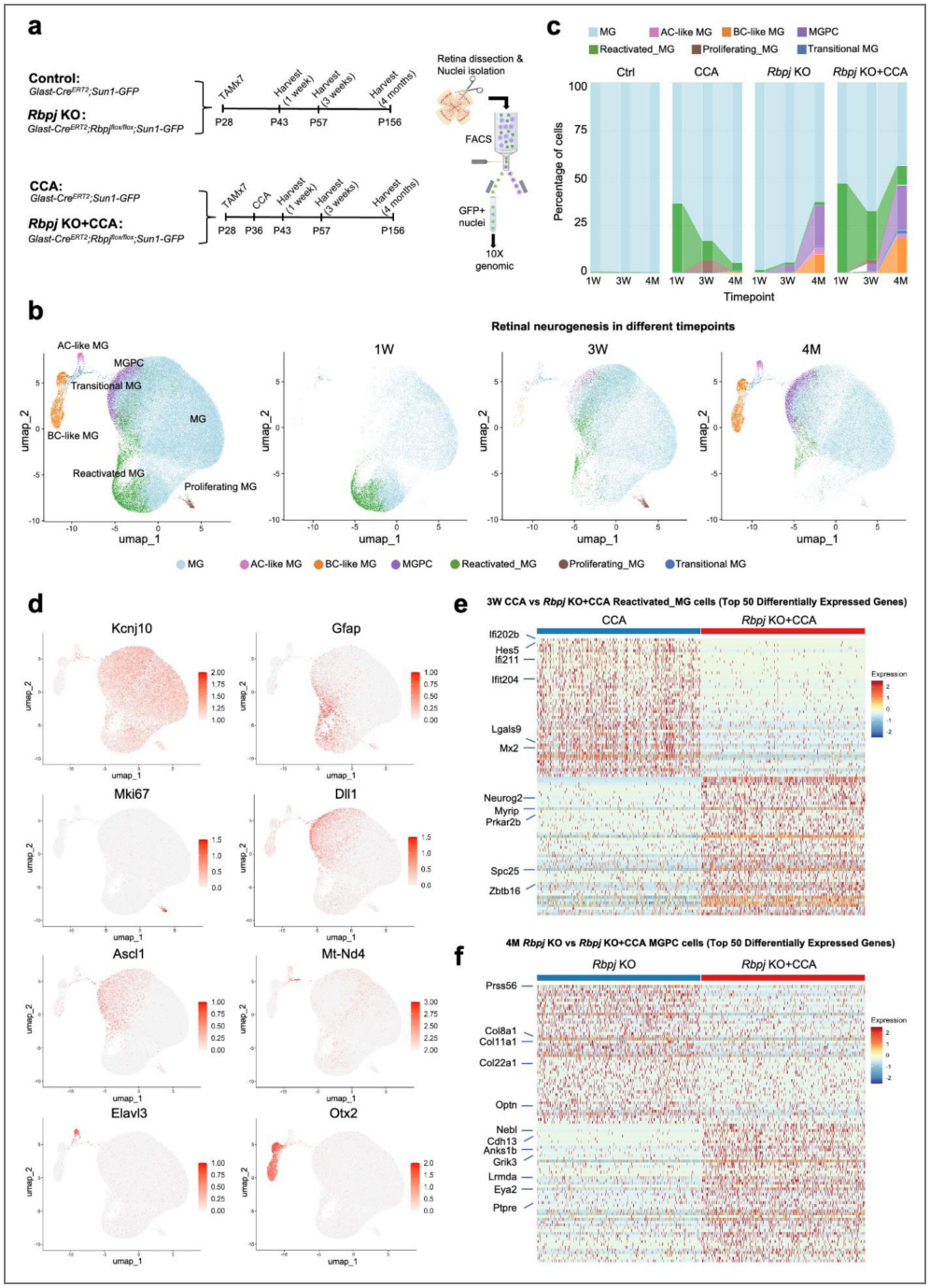

Figure 4. snRNA-seq analysis shows that *Rbpj* KO and CCA promote MG reprogramming.

(a) Schematic illustration of the snRNA-seq experiment. To induce *Rbpj* deletion and GFP expression in MG, we administered TAM for 7 consecutive days in *Glast-Cre^{ERT2};Sun1:GFP* and *Glast-Cre^{ERT2};Rbpj$^{flox/flox}$;Sun1:GFP* mice from P28. At P36, CCA was injected into the CCA and *Rbpj* KO+CCA groups, while control and *Rbpj* KO mice were uninjected by any AAV vector. 3-4 retinas from mice at indicated ages were pooled together for nuclei extraction, and MG nuclei were then isolated by GFP signal via FACS for snRNA-seq. (b) UMAP plot of snRNA-seq data from four treatment groups (Ctrl, CCA, *Rbpj* KO, *Rbpj* KO+CCA) at different timepoints, and separated UMAP based on different timepoints. clusters were identified based on known marker gene expression. (c) Proportions of cell clusters within Ctrl, CCA, *Rbpj* KO and + groups at different timepoints. (d) Feature plots highlighting the cluster of quiescent MG (*Kcnj10*), proliferating MG (*Mki67*), reactivated MG (*Gfap*), MGPC (*Dll1*, *Ascl1*), transitional MG (*Mt-Nd4*), AC-like MG (*Elavl3*), and BC-like MG (*Otx2*). (e) Heatmap showing the expression of top 50 differentially expressed genes (DEGs) of 3-week reactivated MG between CCA and *Rbpj* KO+CCA ($p<0.05$). (f) Heatmap showing the expression of top 50 DEGs of 4-month MGPC between *Rbpj* KO and *Rbpj* KO+CCA ($p<0.05$).

potentially guide reactivated MG back to a quiescent state (Fig. 4e). In contrast, the *Rbpj* KO+CCA-treated reactivated MG cluster demonstrated extensive expression of neurogenic genes, including *Neurog2*, *Zbtb16*, *Myrip*, and *Prkar2b*. (Fig. 4e). *Neurog2* and *Zbtb16* are well-established downstream genes regulated indirectly by the Notch–Rbpj pathway through the pro-neural differentiation programs(38–40). Their upregulation therefore reflects secondary effects of *Rbpj* loss and supports enhanced neurogenic reprogramming in the *Rbpj* KO+CCA group. Interestingly, in *Rbpj* KO+CCA-treated reactivated MG clusters, there was a significant suppression of genes associated with the interferon (IFN) pathway, including *Ifi211*, *Ifit202b*, and *Mx2* (Fig. 4e). As IFN signaling is known to play a crucial role in regulating the plasticity of MG(41–43), its downregulation, coupled with the activation of neurogenic factors, likely catalyzed the formation of MGPCs.

DEG analysis of 4-month MGPC populations revealed distinct transcriptional programs between the *Rbpj* KO and *Rbpj* KO+CCA groups (Fig. 4f). The *Rbpj* KO+CCA MGPCs upregulated genes associated with early retinal progenitor maintenance (*Nebl*, *Eya2*) and retinal development (*Lrmda*, *Ptpre*, *Grik3*) (Fig. 4f). Conversely, the *Rbpj* KO MGPCs preferentially expressed gliosis-related genes, such as *Prss56*, *Optn*, *Col8a1*, *Col22a1*, and *Col11a1* (Fig. 4f)(44–46). Given that retinal gliosis impedes MG reprogramming in mammals(14), these data support the idea that combining *Rbpj* deletion with CCA enhances regenerative potential by boosting early progenitor programs while mitigating the gliotic responses.

CCA promotes BC subtype differentiation of the *Rbpj*-deficient MG

To investigate the heterogeneity of the newly generated neuron, we performed sub-clustering analysis focused specifically on the BC-like cells, which constituted a major reprogrammed neuron-like cluster. Using established BC subtype markers(47), we identified three distinct BC subtypes: OFF-cone BCs (identified by *Pcdh17*, *Zfhx4*, *Lrrtm3*, *Chrm2*), ON-cone BCs (identified by *Isl1*, *Pde8a*, *Esrrg*, *Ryr3*, *Cdh9*, *Grm6*), and rod BCs (identified by *Isl1*, *Prkca*, *Cep112*, *Lrrtm4*) (Fig. 5a-c). Comparative analysis revealed that *Rbpj* deletion and CCA generated a higher abundance of these BC subtypes than either CCA or *Rbpj* deletion treatment alone (Fig. 5d).

To validate the snRNA-seq findings, we performed RNA *in situ* hybridization on *Pcdh17*, *Grm6*, and immunostaining on PKCα to identify OFF-cone BCs, ON-cone BCs, and rod BCs, respectively (Fig. 5e-h). No MG in the control group co-localized with any of these BC markers. The proportions of newborn BC subtypes among MG-derived cells, as quantified by staining, were similar to the proportions observed in the snRNA-seq data (Fig. 5i). Furthermore, some MG-derived neuron-like cells, which are EdU+ Otx2+ tdT+, exhibited morphological changes towards BC, characterized by the retraction of their apical glial processes and the adoption of BC nucleus shapes (Fig. 5j). Collectively, these results indicate that *Rbpj* KO+CCA promoted the generation and maturation of BC subtypes formation.

To better understand the trajectory of neuronal regeneration, we performed pseudotime analysis (Fig. S16a). This revealed a clear and sequential neurogenic order, progressing from resting MG to neurogenic MGPCs, and finally to BC-like and AC-like cells. This progression was closely associated with the downregulation of MG-specific genes (e.g., *Hes5*, *Kcnj10*, *Slc1a2*) and the upregulation of neurogenic factors (e.g., *Neurog2*, *Dll1*, *Eya2*) (Fig. S16b-d). The *Rbpj* KO+CCA treatment group exhibited a more rapid shift in the gene-to-cell ratio trend line towards the BC formation branch compared to the CCA-alone and *Rbpj* KO-alone groups (Fig. S16e), which may explain the increased diversity and abundance of BC-like cells in the *Rbpj* KO+CCA group.

We also investigated whether AC subtypes formed from the MG. Although this cluster could be separated into two distinct sub-clusters, they did not clearly correspond to specific AC subtypes using known marker(48), such as *Chat* for Starburst ACs, *Dab1* for A17 ACs, and *Slc6a9* for nGnG ACs (Fig. S17a). Immunostaining for HuC/D confirmed the formation of AC-like cells, consistent with the snRNA-seq detection (Fig. S17b-c). Quantification further confirmed that the loss of *Rbpj* promotes AC formation compared to the CCA-alone treatment group (Fig. S17d-e).

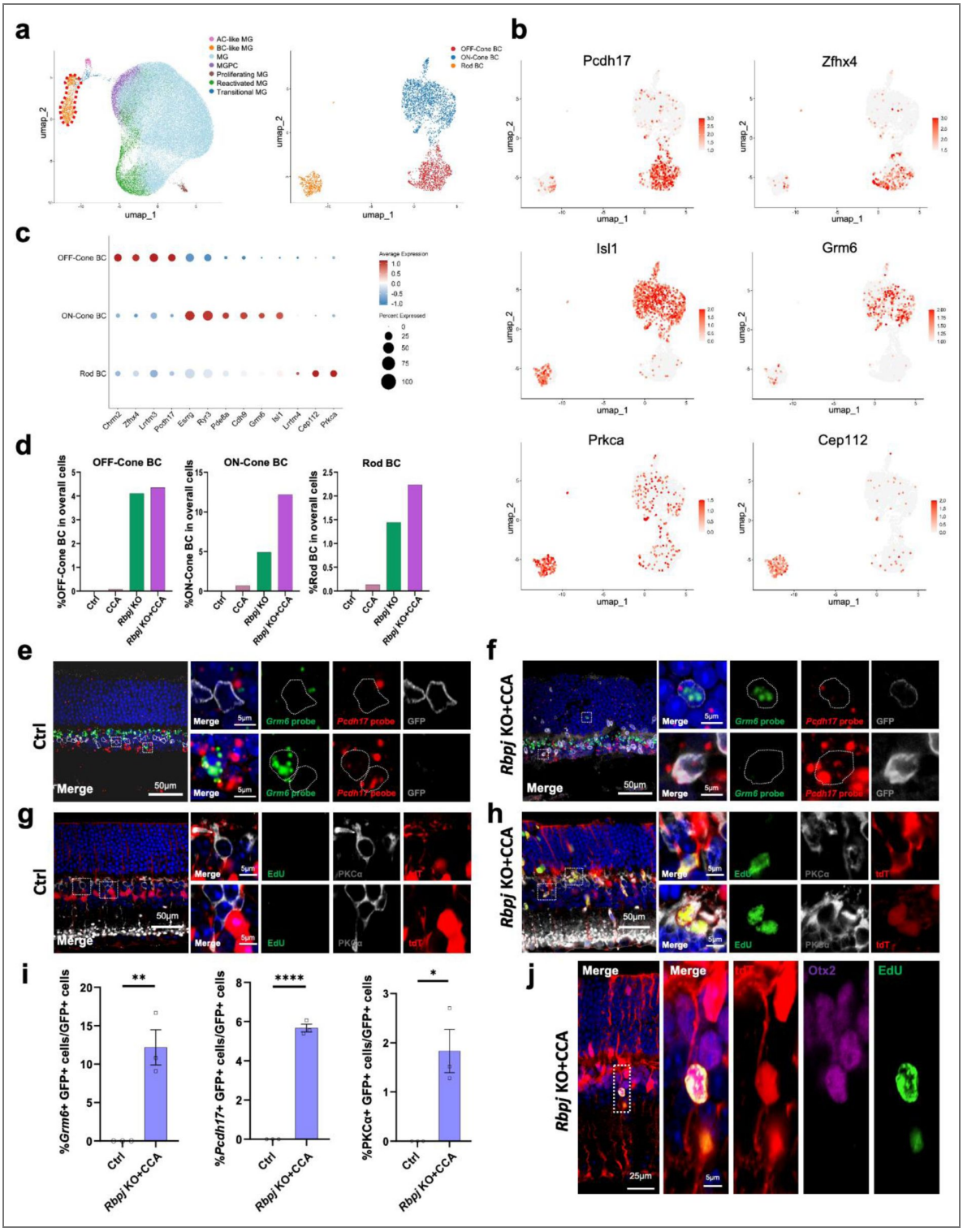

Figure 5. CCA and *Rbpj* deletion drive BC subtype differentiation.

(a) Subclusters of the BC-like population. The BC-like MG (outlined in red) was used for subclustering analysis. (b) Feature plot of BC-like subtypes showing the cluster of OFF-cone BC (*Pcdh17*, *Zfhx4*), ON-cone BC (*Isl1*, *Grm6*) and rod BC (*Isl1*, *Prkca*, *Cep112*). (c) Dot plot showing gene expression and cell percentages for OFF-cone BC, ON-cone BC and rod BC. (d) Percentage of BC subtypes in different treatment groups. (e-f) *Pcdh17* and *Grm6* mRNA *in situ* hybridization in the Ctrl and *Rbpj* KO+OCCA groups. The white dashed boxes indicate the position of the enlarged images. (g-h) Representative immunostaining of EdU and PKCα on retinal sections of the Ctrl and *Rbpj* KO+CCA samples. The white dashed boxes indicate the position of the enlarged images. (i) Percentage showing GFP+ *Grm6*+ cells in overall GFP+ cells, GFP+ *Pcdh17*+ cells in overall GFP+ cells and GFP+ PKCα+ cells in overall GFP+ cells in the Ctrl and *Rbpj* KO+CCA groups. n=3 mice, $*P < 0.05$, $**P < 0.01$, $****P < 0.0001$, by unpaired two-tailed student's t-test. (j) Representative immunostaining of MG-derived cells with bipolar cell morphology.

While the neuron-like clusters were best classified as BC-like and AC-like based on their distinct marker gene expression, they also exhibited mixed expression of genes associated with other retinal neuronal types, including RGC markers (e.g., *Tubb3*, *Myt1l*, *Grin1*) and photoreceptor markers (e.g., *Crx*, *Prom1*, *Epha10*, *Gucy2e*, *Scg3*) (Fig. S18a), suggesting that the regenerated cells exist in a hybrid state. Notably, we did not detect Nrl expression in the newborn neuron clusters, which is essential for rod photoreceptor specification(37) (Fig. S18a). The discrepancy in Nrl detection between snRNA-seq and prior immunofluorescence staining suggests that Nrl+ cell generation is stochastic and occurs at low frequency (Fig. S12b–c, Fig. S18a). Moreover, relative to the *Rbpj* KO group, neuron-like clusters in the *Rbpj* KO+CCA group showed upregulated expression of genes typically enriched in both RGCs and photoreceptors, such as *Tmem132d*, *Cntn5*, *Ryr2*, *Mef2c*, *Meis2*, and *Cngb1* (Fig. S18b). Together, these mixed lineage signatures indicate that the newly generated neurons remain in a plastic, incompletely committed state and likely require additional cues, such as Nrl, to achieve full maturation and terminal specification. Moreover, combining *Rbpj* deficiency with CCA treatment enhances the acquisition of abundant and distinct neuronal characteristics in the newborn neurons.

Increased chromatin accessibility of neurogenic factors underlies CCA-induced neuronal formation from MGPCs

We next sought to elucidate how CCA promotes neurogenesis. We hypothesized that CCA-induced MG proliferation remodels the chromatin landscape to facilitate reprogramming, a mechanism analogous to those observed in somatic cell reprogramming and cardiac regeneration(49, 50). To test this hypothesis, we profiled chromatin accessibility using snATAC-seq on MG nuclei purified from four groups at 4 months post-treatment, including the untreated control, CCA, *Rbpj* KO, and the combined *Rbpj* KO+CCA group (Fig. 6a).

No batch effects were detected across treatments, and clusters were annotated using canonical cell type-specific markers (Fig. S19a–c). After quality control and removal of native mature neurons, which uniformly represented across groups, approximately 8,000–11,000 cells remained for downstream analysis (Fig. 6b–c). Clustering resolved six cell types based on marker accessibility: resting MG, active MG, *Rbpj* KO MG (KO MG), MGPC, AC-like, and BC-like, with distinct compositional shifts across treatments (Fig. 6b–c). As expected, MG in the control group exhibited a quiescent chromatin state, with high accessibility at classic MG marker genes (e.g., *Kcnj10*, *Rlbp1*, *Aqp4*) (Fig. 6d-e). A unique active MG cluster, showing markedly increased accessibility at loci involved in cell cycle regulation (e.g., *Firre*, *Cdc45*, *Bcl3*), was characterized in the CCA treated group (Fig. 6d-e). In *Rbpj* deficient MG, accessibility at Notch pathway effectors (*Hes1*, *Hes5*, *Heyl*) was markedly reduced relative to resting MG (Fig. 6d–e). Notably, the *Rbpj* KO+CCA combination produced more pronounced chromatin changes associated with MGPC, AC-like, and BC-like states compared to *Rbpj* KO alone, underscoring the contribution of CCA to chromatin remodeling (Fig. 6d–e).

A direct comparison of resting MG versus active MG within the CCA treatment group revealed broad increases in chromatin accessibility (Fig. 6f), with upregulated loci linked to retinal development and neurogenesis, including *Neurod2*, *Dll1*, and *Otx2* (Fig. 6f). WikiPathways enrichment indicated strong associations with dopaminergic neurogenesis (Fig. 6g). Genome browser tracks further showed elevated accessibility across the *Neurod2* promoter and gene body in active MG relative to resting MG, consistent with the activation of this key neurogenic regulator (Fig. 6h).

In summary, our snATAC-seq data support a model wherein CCA-induced proliferation remodels the chromatin landscape of MG, priming them for reprogramming by opening key neurogenic loci.

MG-derived daughter cells exhibit long-term survival

To evaluate long-term outcomes of MG reprogramming, a cohort of mice treated with *Rbpj* KO and CCA were aged to 9 months post-treatment (Fig. 7a). At this late time point, MG-derived cells, marked by the tdT reporter, displayed a more regular, circular nuclear morphology reminiscent of

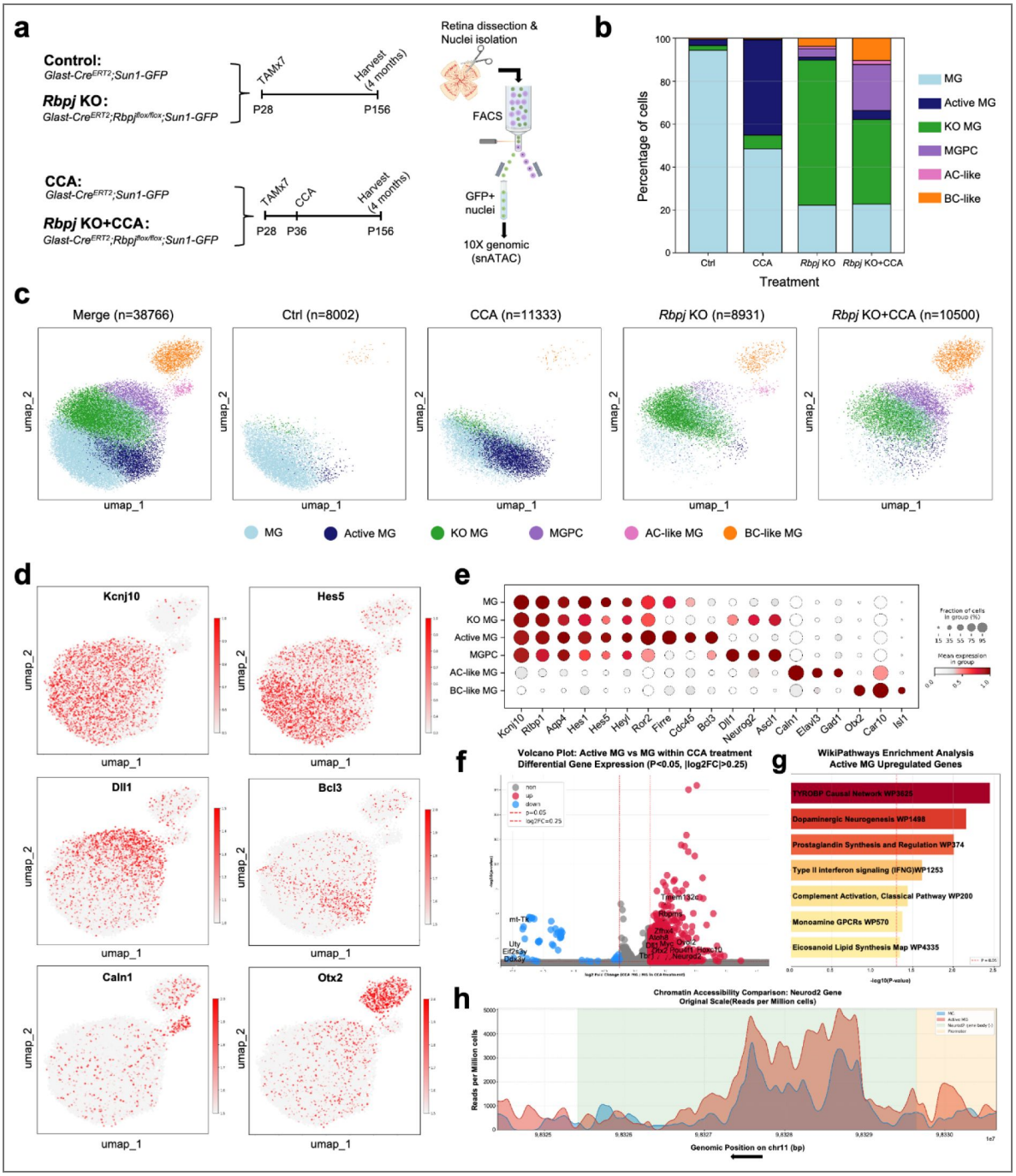

Figure 6. snATAC-seq analysis suggests increased chromatin accessibility of the neurogenic genes by CCA.

(a) Schematic illustration of the snATAC-seq experiment. (b) Proportions of cell clusters within Ctrl, CCA, *Rbpj* KO and *Rbpj* KO+CCA groups. (c) UMAP plot of snATAC-seq data from four treatment groups (Ctrl, CCA, *Rbpj* KO, *Rbpj* KO+CCA). (d) Feature plots highlighting the cluster of quiescent MG (Kcnj10), KO MG (Hes5), active MG (Bal3), MGPC (Dll1), AC-like MG (Caln1), BC-like MG (Otx2). (e) Dot plot showing gene expression and cell percentages for quiescent MG, KO MG, active MG, MGPC, AC-like MG, BC-like MG. (f) Volcano plot showing the differential gene expression of MG and active MG within CCA treatment group ($p<0.05$). Red dots indicate the genes upregulated in active MG and blue dots indicate genes downregulated in active MG. (g) WikiPathways enrichment analysis of upregulated genes in active MG ($p<0.05$). (h) Increased chromatin accessibility at the Neurod2 locus was observed in the active MG. The black arrow shows the transcription direction.

mature retinal neurons, though fully mature rod photoreceptors were not detected (Fig. 7b). Quantification showed an upward trend in the proportion of Otx2+ tdT+ cells among total tdT+ cells, consistent with a gradual, ongoing MG-to-neuron reprogramming process (Fig. 7b-c). However, both the percentage of Otx2+ EdU+ tdT+ cells within the EdU+ tdT+ population and the absolute number of EdU+ cells declined slightly over time (Fig. 7d–e). This data suggests that while most MG-derived daughter cells persist long-term, a small subset of proliferated MG-derived neurons may ultimately undergo apoptosis. To evaluate retinal structure following treatment, we performed ZO1 staining to visualize the outer limiting membrane (OLM) (Fig. S20a). The OLM integrity in the *Rbpj* KO+CCA group at 9 months was comparable to that of untreated controls, suggesting that sufficient MG persist to support junctional complexes (Fig. S20b). This finding indicates that combined *Rbpj* KO and CCA treatment achieves neurogenesis without compromising the essential supportive functions of MG or retinal homeostasis.

In summary, our findings demonstrate that the majority of MG-derived cells possess inherent long-term stability, and that maintaining an adequate MG population is a prerequisite for achieving stable and functional regeneration.

Discussion

Retinal degeneration is characterized by the progressive loss of retinal neurons, leading to irreversible vision impairment. In teleost fish, retinal injury triggers functional regeneration, with MG serving as the source of regenerated neurons. In contrast, adult mammalian retinas lack regenerative capacity because MG fail to re-enter the cell cycle, dedifferentiate, and subsequently differentiate into neurons. In our previous study, we showed that simultaneous knockdown of $p27^{Kip1}$ and overexpression of cyclin D1 effectively drives mouse MG to re-enter the cell cycle in the absence of injury. However, most postmitotic MG underwent only transient dedifferentiation, and only a small fraction (~1%) differentiated into neuron-like cells(10). In the present study, scRNA-seq and RNA *in situ* hybridization revealed persistent activation of Notch signaling in postmitotic MG, which restricts their reprogramming potential. Conditional deletion of *Rbpj*, the core transcriptional effector of Notch signaling, in late-stage RPCs promoted ectopic rod photoreceptor formation at the expense of MG differentiation, whereas *Rbpj* deletion in mature MG alone produced only limited neurogenic effects, suggesting that epigenetic landscape changes may contribute to more limited reprogramming potential from late RPC-to-MG transition. Notably, combining *Rbpj* knockout with the proliferative stimulus CCA treatment markedly enhanced neurogenesis from postmitotic MG. Immunofluorescence showed that ~26% of MG daughter cells expressed neuronal marker Otx2 and HuC/D. snRNA-seq confirmed these results and revealed a clear trajectory of MG-derived neurogenesis, in which cells transitioned from a glial state toward BC-like and AC-like identities. Subtype analysis identified three BC subtypes: OFF-cone BCs, ON-cone BCs, and rod BCs, among MG-derived BC-like cells, whereas AC-like cells could not be further classified. MG-derived neuron-like cells also expressed genes characteristic of RGCs and photoreceptors, indicating enhanced lineage promiscuity. This hybrid transcriptomic profile, together with the immature morphology of newborn neurons, suggests incomplete or inefficient reprogramming. Mechanistically, snATAC-seq revealed that CCA treatment increases chromatin accessibility at pro-neurogenic loci following MG proliferation, likely facilitating the improved reprogramming efficiency of *Rbpj*-/- MG. Notably, the majority of reprogrammed neurons survived for up to 9 months, while the MG pool remained intact, underscoring their preserved function to support retinal homeostasis.

MG are essential for maintaining retinal structural and functional integrity. They contribute to the blood-retinal barrier, regulate extracellular ion and neurotransmitter homeostasis, provide metabolic support to neurons, and mediate inflammatory responses(51, 52). Thus, preserving MG number and function during reprogramming interventions is critical, as extensive MG loss or dysfunction of MG could disrupt retinal homeostasis and exacerbate degeneration(17). In zebrafish, MG regenerate neurons through asymmetric division, generating one self-renewing MG and one progenitor cell, thereby maintaining the glial pool(53, 54). In our study, combined CCA treatment and *Rbpj* deletion effectively stimulated MG proliferation and reprogramming in the

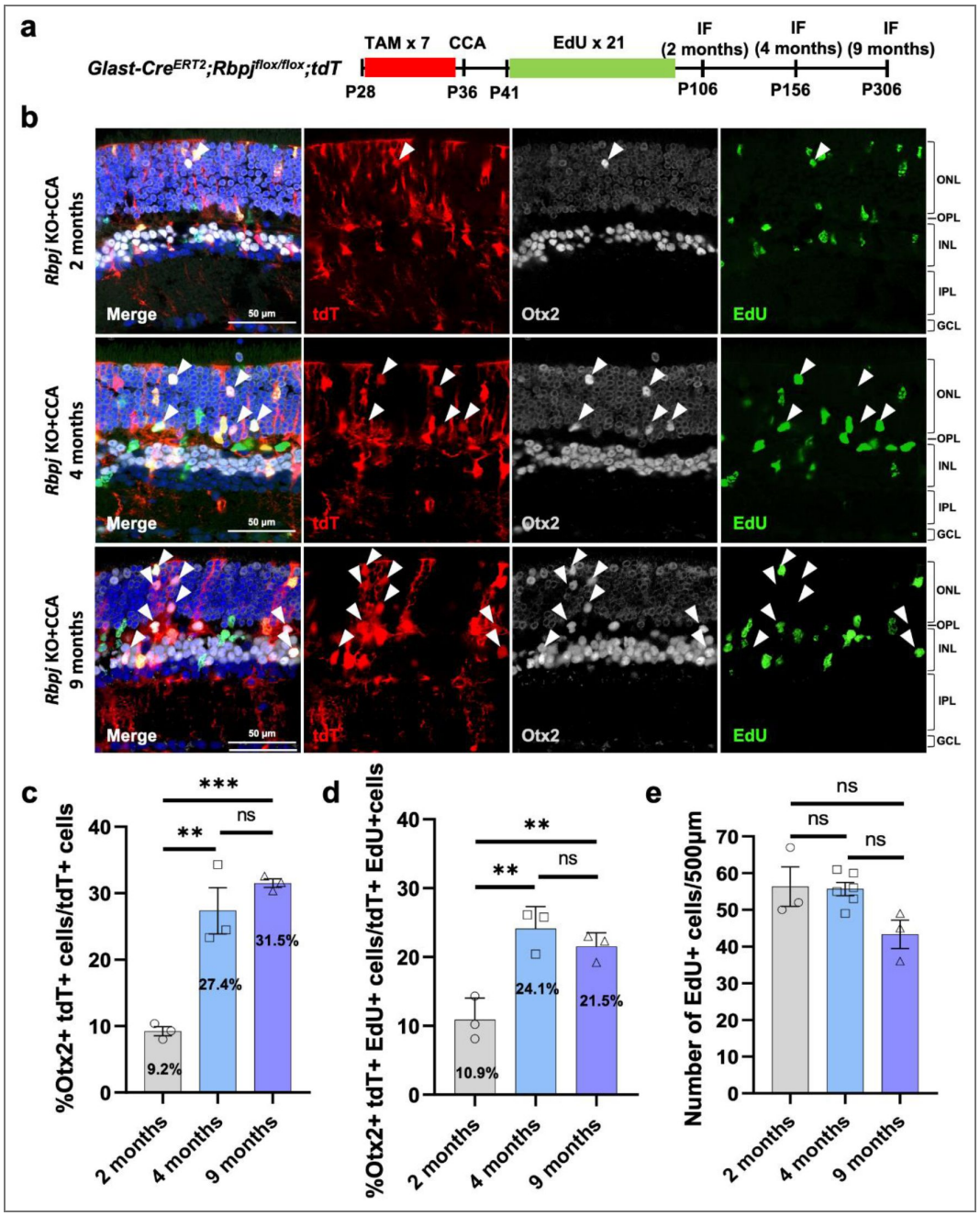

Figure 7. Neurons derived from MG exhibited long-term survival capabilities.

(a) Schematic illustration of the experiment assessing long-term cell survival. (b) Representative immunostaining of EdU and Otx2 on retinal sections. The white arrows refer to tdT+ Otx2+ cells. (c) Percentage of tdT+ Otx2+ cells in overall tdT+ cells, n=3 mice, data are presented as mean ± SEM. ns=not significant, $^{**}P < 0.01$, $^{***}P < 0.001$, by one-way ANOVA with Tukey's post hoc test. (d) Percentage of tdT+ EdU+ Otx2+ cells in overall tdT+ EdU+ cells, ns=not significant, $^{**}P < 0.01$, by one-way ANOVA with Tukey's post hoc test. (e) Number of EdU+ cells per 500 μm, ns=not significant, by one-way ANOVA with Tukey's post hoc test.

adult mouse retina without overt MG depletion. Because both daughter cells lacked *Rbpj*, a classic asymmetric division with one daughter have high Notch signaling and the other low is unlikely. Nonetheless, our strategy successfully regenerated neuron-like cells while maintained the MG pool, as more MG were generated to replace the reprogrammed MG. The long-term survival of newborn neurons and the stability of retinal architecture support the integrity of the MG pool. Although our strategy differs from zebrafish MG self-renewal, it still offers a viable regenerative approach that preserves glial homeostasis, a critical prerequisite for maintaining retinal homeostasis. Achieving a balance between neurogenesis and MG preservation represents a central challenge in glial-based regeneration. Excessive or widespread reprogramming risks depleting MG below a critical threshold or impairing their supportive functions. Future strategies should emphasize transient, partial, or spatially confined reprogramming to maintain a functional MG pool. For instance, replication-incompetent retroviral vectors(55, 56) to knockout *Rbpj* in one daughter cell of a divided MG could ensure that the sibling cell remains a supportive glial cell, thereby maintaining retinal homeostasis while generating new neurons.

Multiple studies have explored the proliferative potential of MG in adult mice, including Wnt pathway activation, Hippo pathway inhibition, and forced manipulations of cell cycle regulators(10–12). However, unlike zebrafish, proliferating mouse MG rarely give rise to mature retinal neurons, regardless of the proliferation-inducing method. Our time-course snRNA-seq analysis of CCA-treated retinas confirmed this limitation: MG re-entered and exited the cell cycle but largely reverted toa quiescent glial state. So, what is the functional role of MG proliferation in retinal regeneration? Our findings imply that proliferation actively facilitates reprogramming rather than merely expanding MG numbers. In *Rbpj*-deficient MG, proliferation enhanced neuronal gene expression. This principle parallels findings in somatic cell reprogramming, where cell division rate is directly proportional to reprogramming efficiency and it facilitates the acquisition of epigenetic marks that help re-establish the core transcriptional circuitry for pluripotency(50, 57–59). Similarly, proliferative neural stem cells (NSCs) exhibit higher chromatin accessibility at pro-neural genes Otx2 and Ascl1, compared with aged NSCs that show reduced proliferative capacity(60, 61). Enhancing NSCs proliferation with betacellulin upregulated Ascl1 and Nestin, thereby boosting neurogenesis in the olfactory bulb and dentate gyrus(62). Our findings provided supportive evidence that proliferation-enhanced reprogramming efficiency may be conserved in MG. Moreover, we show that CCA-induced proliferation triggers widespread chromatin opening at neurogenic gene loci in MG (Fig. 6f–h), which may underlie the superior reprogramming efficiency and enhanced generation of BC subtypes, as well as the upregulation of genes linked to photoreceptors and RGCs, compared with *Rbpj* deletion alone.

The Notch signaling pathway plays a pivotal role in regulating both cell proliferation and cell fate specification throughout retinal development(31, 32). During development, Notch-mediated lateral inhibition ensures that diverse retinal cell types are generated in a spatially and temporally coordinated manner. Deletion of Notch1 or downstream effectors such as *Hes1* and *Rbpj* disrupts this balance, causing premature cell-cycle exit of retinal progenitor cells and increased production of early-born neurons, particularly photoreceptors, at the expense of later-born cell types, including MG(31, 63). Conversely, forced expression of *Hes1* in progenitor cells drives gliogenesis and promotes MG differentiation(64). Align with this paradigm, *Rbpj* deletion during retinal development redirected the fate of late-stage progenitor cells, producing more mature rod photoreceptors at the expense of MG and BCs. In the mature retina, sustained Notch signaling maintains MG quiescence(14, 26). Its conserved role across species has been well documented: inhibition of the Delta-Notch3-Hey1/Id2b pathway triggers zebrafish MG proliferation and regeneration(18, 65, 66). In the post hatch chick retina, Notch inhibition using a γ-secretase inhibitor likewise enhances retinal regeneration(67). In adult mice, simultaneous suppression of Notch signaling and deletion of Nfia/b/x synergistically promotes MG conversion into BCs and ACs(25). Similarly, virus-mediated Oct4 overexpression combined with Notch inhibition boosts the neurogenic competence of mammalian MG(24). Collectively, these findings position Notch inhibition as a central mechanism for unlocking MG plasticity. Together, these studies highlight Notch inhibition as a critical gatekeeper of MG plasticity. However, both our work and others indicate that Notch inhibition primarily generates BC- and AC-like neurons, with limited evidence

for mature photoreceptor formation. This underscores an enduring barrier to producing the full repertoire of retinal neurons and suggests that additional lineage determinants, such as Nrl, may be required to guide MG toward photoreceptor fates.

Regenerating retinal neurons from endogenous MG represents a promising frontier in regenerative medicine, yet the long-term survival of newly generated neurons is essential for clinical translation. Normally, mature retinal neurons depend on intrinsic survival mechanisms and extrinsic trophic support from the microenvironment, including trophic factors, such as brain-derived neurotrophic factor (BDNF), ciliary neurotrophic factor (CNTF), glial cell-line derived neurotrophic factor (GDNF) and nerve growth factor (NGF), synaptic integration for functional activity-dependent survival, and metabolic support from the RPE, and vasculature(68, 69). In contrast, transplanted neurons often suffer low survival rate due to poor migration, inadequate support, limited synaptic integration, and immune rejection(70–72). For example, xenotransplantation of mouse induced pluripotent stem cell/mouse embryonic stem cell-derived RGCs exhibit only minimal medium-term survival in the host retina owing to immune barriers(70–72). While the survival of endogenous MG-derived neurons has been under explored, our study demonstrates a remarkably high long-term survival rate, with ~80% of postmitotic MG-derived newborn neurons persisting for at least 9 months following combined *Rbpj* deletion and CCA treatment. We speculate that it may involve successful apical migration to their appropriate retinal layers (e.g., ONL and INL), where they can access layer-specific trophic support and integrate into local microenvironments. Their laminar positioning likely facilitates contact with presynaptic and postsynaptic partners, as well as access to survival signals from MG and photoreceptor cells, which are critical for preventing apoptosis. To further enhance the survival of newborn neurons from MG, future strategies should focus on recapitulating the endogenous survival mechanisms of the retina. This could involve co-expression of anti-apoptotic genes such as *Bcl-2* or *Xiap*(73, 74) and supplemental trophic support (e.g., BDNF, CNTF), alongside synaptic integration through molecular guidance cues such as Semaphorins or Netrins(75, 76). Regenerating neurons within a degenerating retinal environment, where vacated synaptic positions may facilitate new connections, may further enhance neuronal integration. The efforts to enhance the survival of regenerated neurons will be essential for advancing regenerative therapies.

Materials and Methods

Animals

Rbpj$^{flox/flox}$ mice (strain: *Rbpj*^{em2Lutzy}), *tdTomato* reporter mice (strain *B6.Cg-Gt(ROSA)26Sor*$^{tm14(CAG-tdTomato)Hze}$*/J*)(77), *Sun1:GFP* reporter mice (Strain *B6.129-Gt(ROSA)26Sor*$^{tm5.1(CAG-Sun1/sfGFP)Nat}$*/MmbeJ*)(78), and *Glast-Cre*^{ERT2} reporter mice (strain *Tg(Slc1a3-cre/ERT)1Nat/J*)(79) mice were purchased from the Jackson Laboratory. All mice were kept on a 12/12-hour light/dark cycle in the Laboratory Animal Research Unit, City University of Hong Kong. All animal procedures performed were approved by the Hong Kong Department of Health under Animals Ordinance Chapter 340 (Ref: (20–130) in DH/HT&A/8/2/5 Pt.2) and by the City University of Hong Kong Animal ethics committee (Ref: A-0264).

AAV Production

AAV production was carried out following the previously described procedure (80). In brief, to produce the recombinant AAV$_{7M8}$-GFAP-cyclinD1-p27^{Kip1} shRNA-WPRE, the HEK293T cells were transfected with a mixture of pAAV-GFAP-cyclinD1-p27^{Kip1}nshRNA-WPRE vector transgene plasmid, rep/cap packaging plasmid and adenoviral helper plasmid. At 96 hours post-transfection, both the culture medium and the transfected cells were harvested for AAV collection. The collected AAV underwent further purification through ultra-centrifugation in the iodixanol (OptiPrep) gradient at 147,000 x g at 4°C for 90 minutes. The iodixanol in the AAV solution was washed three times with PBS using Amicon 100K columns (EMD Millipore), and about 30μl of the final volume AAV was collected for downstream applications. The virus titration was determined through the protein SDS-PAGE method.

Tamoxifen injection

To induce Cre recombinase expression in the majority of MG, tamoxifen (Sigma, dissolved in corn oil) was administered via intraperitoneal injection at a dosage of 50mg/kg.

Intravitreal AAV injection

To stimulate MG proliferation, mice were intravitreally injected with AAV_{7m8}-GFAP-cyclinD1-$p27^{Kip1}$ shRNA-WPRE at a final concentration of 4E13vg/ml. Briefly, the eyelid was gently manipulated with tweezers to expose the eyeball. Subsequently, 1μl of the virus was precisely introduced into the intravitreal space using a custom angled glass pipette controlled by a FemtoJet (Eppendorf). The treatment was administered to the right eye of the animal, while the left eye remained untreated as a control.

Retinal Cryosection and Immunohistochemistry

The mice were humanely euthanized using CO_2 and cervical dislocation. Before enucleation, the eyeballs were marked ventrally to indicate the AAV injection site, and then the retinas were carefully dissected in PBS and fixed in 4% paraformaldehyde (PFA) at room temperature for 30 minutes. The fixed retinas underwent three-times washes with PBS (Product #10010023, Thermo Fisher Scientific) and were subsequently dehydrated in sequential sucrose solutions of 5%, 15%, and 30% for 15, 30, and 60 minutes, respectively. The retina was then immersed in a solution of optimal cutting temperature (OCT) and 30% sucrose in a 1:1 ratio at 4°C overnight before being embedded in cryomolds in a specific orientation for sectioning.

After freezing the tissue below -20°C, a series of 20μm sections were cut and mounted on glass slides using a cryostat machine (Thermo HM525NX Cryostat). For immunostaining, retinal sections were first blocked in 3% bovine serum albumin (BSA, #A9647, Sigma-Aldrich) and 0.1% Triton X-100 in PBS (PBST) for 30 minutes at room temperature, followed by overnight incubation with primary antibodies at the recommended dilution at 4°C. Primary antibodies used in this study included goat anti-Otx2 antibody (1:200, AF 1979; R&D systems), mouse anti-HuC/D (1:200, A21271; Thermo Fisher Scientific), rabbit anti-Sox9 antibody (1:500, AB5535; Millipore), rabbit anti-mCAR (1:200, AB15282, Millipore), rabbit anti-Nrl (1:150, AF2945, R&D Systems), mouse anti-PKCα (1:200, sc-8393, Santa Cruz), rabbit anti-Crx (1:500, PA5-32182, Thermo Fisher Scientific), goat anti-Sox2 (1:500, AF2018, R&D Systems), rabbit anti-Pax6 (1:500, AB2237, Millipore), rabbit anti-ZO1 (1:500, 61-7300, Thermo Fisher Scientific), rabbit anti-Rbpms (1:500, ab152101, Abcam). Following primary antibody incubation, the samples were washed thrice with PBST before incubation with a mixture of DAPI (0.5μg/ml) and secondary antibodies in the dark for 2 hours at room temperature.

Subsequently, the retinal sections were washed and mounted with an anti-fade solution before microscopy or storage. Slide images were captured using sing Nikon A1HD25 High speed and Large Field of View Confocal Microscope. Histological measurements and image processing were conducted using ImageJ software.

EdU Incorporation and Detection

5'-ethynyl-2'-deoxyuridine (EdU, 50mg/kg, Abcam ab146186) was intraperitoneally injected for 21 days after CCA administration to label the cells in the S phase. EdU staining was performed following the instruction of the Click-iT™ EdU Alexa Fluor™ 488 or 647 Imaging Kit (C10337, Thermo Fisher Scientific).

In situ RNA hybridization

In the study, *in situ* RNA hybridization was conducted utilizing the RNAscope Multiplex Fluorescent Detection Reagents V2 kit (Advanced Cell Diagnostics) following standard commercial procedures. Initially, retinas were carefully dissected, fixed in 4% PFA, dehydrated using a sucrose solution, and embedded in OCT medium. Subsequently, the retinas were sectioned into 20μm slices and placed on SuperFrost Plus glass slides (Epredia). After removing the OCT with PBS and dehydrating further with 50%, 70% and 100% ethanol, the retinal sections were incubated with a

GFP antibody (AB_2307313; Aves Labs) overnight at 4°C. Post a triple wash with PBST (PBS with 0.1% Tween-20), the sections were hybridized with RNA probes: *Hes1* probe (Cat No.417701-C2 RNAscope™ Probe-Mm-*Hes1*-C2), *Pcdh17* probe (Cat No.489901-C2 RNAscope™ Probe-Mm-*Pcdh17*-C2) and Grm6 probe (Cat No.511611 RNAscope™ Probe-Mm-*Grm6*) for 2 hours at 40°C. Following the RNA hybridization process, the slides were stained with secondary antibodies (Jackson ImmunoResearch) and DAPI for two hours at room temperature.

The resulting fluorescent signals were observed and captured using a Nikon A1HD25 High-Speed and Large Field of View Confocal Microscope. The mRNA levels within the GFP-labeled nuclei membrane were then quantified by measuring the signal intensity level using ImageJ.

MG sorting and snRNA library preparation and sequencing

Three or four fresh retinas were dissected from adult mice (strain: *Glast-Cre^{ERT2};Rbpj$^{flox/flox}$;Sun1:GFP* and *Glast-Cre^{ERT2};Sun1:GFP*, aged as specified in Results) under RNase-free conditions in cold PBS on ice to minimize RNA degradation. Dissection tools (forceps, scissors) were sterilized with 70% ethanol and RNase Zap (Product #AM9780, Thermo Fisher Scientific) to eliminate RNase contamination. Retinas were frozen in liquid nitrogen until use. Retinal tissues were homogenized in 500μL of ice-cold NP-40 lysis buffer (Product #74385, Sigma-Aldrich) supplemented with 1× protease inhibitor cocktail (Product #P8340, Sigma-Aldrich) and 1U/μL RNase inhibitor (Product #EO0381, Thermo Fisher Scientific) using a pellet pestle (AST-YMB-15, Axyste). Homogenization was performed on ice with 15–20 gentle strokes to avoid excessive shearing of nuclei, followed by incubation on ice for 5 minutes to ensure complete lysis of cytoplasmic membranes while preserving nuclear integrity. The homogenate was filtered through a 70μm MACS® SmartStrainer (Catalog #130-110-915, Miltenyi Biotec) pre-rinsed with cold PBS to remove cell debris and intact cells. The filtrate (containing nuclei) was centrifuged at 500 × g for 5 minutes at 4°C to pellet nuclei, and the supernatant was discarded. The nuclear pellet was resuspended in 1mL of 1% BSA in PBS (1% BSA-PBS), supplemented with 1U/μL RNase inhibitor, to neutralize residual lysis buffer and stabilize nuclei. To enrich for MG nuclei (a rare population comprising 2–3% of total retinal cells), fluorescence-activated cell sorting (FACS) was performed using a Sony SH800Z cell sorter equipped with a 488-nm laser for GFP excitation and a 525/50-nm emission filter. Nuclei were gated based on forward scatter (FSC) and side scatter (SSC) to exclude debris and aggregates, and GFP-positive events were sorted into RNase-free 1.5mL tubes containing 100μL of 1% BSA-PBS with RNase inhibitor. Sorting was performed at 4°C with a flow rate of 1,000–2,000 events/second. Approximately 200,000 GFP+ nuclei were collected per sample and centrifuged at 500 × g for 5 minutes at 4°C. The pellet was resuspended in 1% BSA-PBS (with RNase inhibitor) and adjusted to a concentration of 600–800 nuclei/μL using a Countess II FL Automated Cell Counter (Thermo Fisher Scientific), ensuring compatibility with 10x Genomics Chromium systems for optimal Gel Bead-in-Emulsion (GEM) formation.

snRNA sequencing libraries were prepared using the Chromium Next GEM Single Cell 3' GEM, Library & Gel Bead Kit v3.1 (Catalog #1000269, 10x Genomics), Chromium Next GEM Chip G Single Cell Kit (Catalog #1000127, 10x Genomics), and Chromium Controller iX. Briefly, 20μL of the nuclei suspension (containing ~18,000 nuclei) was loaded into a well of the Chromium Next GEM Chip G, along with reverse transcription (RT) reagents, gel beads, and partitioning oil. GEMs were generated using the Chromium Controller iX, with each GEM containing a single nucleus, a gel bead (with barcoded oligonucleotides), and RT reagents. GEMs were transferred to 0.2-mL 8-tube strips (951010022, Eppendorf) and subjected to RT in a ProFlex™ PCR System (4484073, Thermo Fisher Scientific) with the following program: 53°C for 45 minutes, 85°C for 5 minutes, and hold at 4°C. Resulting cDNA was amplified using 11 cycles of PCR (98°C for 3 minutes; 12 cycles of 98°C for 15 seconds, 63°C for 20 seconds, 72°C for 1 minute; final extension at 72°C for 1 minutes) to generate sufficient material for library construction. Amplified cDNA was purified using SPRIselect beads (Beckman Coulter) at a 1:1.8 ratio (cDNA:beads) to remove primers and impurities. Purified cDNA was fragmented enzymatically (32°C for 5 minutes) using the

Fragmentation Enzyme Mix (included in the 10x kit), followed by end repair, A-tailing, and ligation of Illumina-compatible adapters. Final libraries were purified with SPRIselect beads (1:1 ratio) and quantified using a Qubit 4 Fluorometer (Thermo Fisher Scientific).

Libraries were sequenced by Novogene (Beijing) on an Illumina NovaSeq 6000 platform using paired-end 150-bp reads. Each sample was allocated 100 Gb of sequencing data, ensuring an average depth of ~35,000 reads per nucleus to capture robust transcriptomic profiles, including low-abundance transcripts relevant to MG function and differentiation. This expanded method provides detailed, reproducible parameters for each step, including reagent supplements, centrifugation conditions, FACS gating, and sequencing metrics, to support rigorous replication of the experiment.

Preprocessing, filtering and clustering of snRNA data

The raw sequencing reads (paired-end 150 bp) were processed using Cell Ranger software (v6.1.2, 10x Genomics) following the manufacturer's recommended pipeline (*https://support.10xgenomics.com/single-cell-gene-expression/software/pipelines/latest/what-is-cell-ranger*). For each sample, count was used to align reads to the mouse reference genome (mm10/GRCm38) and quantify gene expression. Cell Ranger's built-in quality control metrics were used to generate filtered matrices, excluding potential cell-free RNA or debris-associated barcodes.

Subsequently, quality control, filtering, dimensional reduction, and clustering of the data were performed utilizing the Seurat package in R (81). Doublets and cells with less than 200 or more than 6000 expressed features and a percentage of mitochondrial transcripts exceeding 20% were excluded from further analysis. For the remaining cells, UMAP dimension reduction based on eight principal components (PCs) was implemented, and cells were clustered using the graphical clustering method within Seurat. Cell types were identified by leveraging known marker genes.

snATAC library preparation and sequencing

Retinal MG nuclei were isolated as described in the snRNA-seq library preparation section. To permeabilize nuclear membranes for chromatin accessibility, isolated nuclei were treated with lysis buffer containing 5% digitonin (Thermo Fisher Scientific) for 1 minute on ice, then immediately washed and resuspended in diluted Nuclei Buffer (prepared by diluting 20X Nuclei Buffer, PN-2000207, 1:20 in nuclease-free water) to a final concentration of approximately 4,000 nuclei/μL.

snATAC-seq libraries were generated using the Chromium Next GEM Single Cell ATAC Kit v2 (PN-1000406, 10x Genomics) following the manufacturer's protocol (CG000496 Rev C). In brief, permeabilized nuclei were incubated with Transposition Mix (ATAC Buffer B and ATAC Enzyme B) at 37°C for 30 minutes. Transposed nuclei were mixed with Master Mix (Barcoding Reagent B, Reducing Agent B, Barcoding Enzyme) and loaded onto a Chromium Chip H with ATAC Gel Beads v2 and Partitioning Oil to form GEMs using the Chromium Controller iX. GEMs were thermocycled (72°C 5 min; 98°C 30 sec; 12 cycles of 98°C 10 sec, 59°C 30 sec, 72°C 1 min; hold 15°C). Post-GEM cleanup used Dynabeads MyOne SILANE followed by double-sided SPRIselect purification. Indexed libraries were PCR-amplified for 7 cycles and purified again with SPRIselect. Library quality was assessed using an Agilent 2100 Bioanalyzer and sequenced by Novogene on an Illumina NovaSeq 6000 (PE150), with 120 Gb generated per sample.

Preprocessing, Filtering and Clustering of snATAC-seq Data

The raw sequencing reads (paired-end 150 bp) were processed using Cell Ranger ATAC software (10x Genomics) following the manufacturer's recommended pipeline. The workflow included: Illumina BCL files were converted to FASTQ format using cellranger-atac mkfastq, which assigned reads to individual samples based on index barcodes. For each sample, cellranger-atac count was used to align reads to the mouse reference genome (mm10/GRCm38) and generate fragment files quantifying chromatin accessibility.

Subsequently, quality control, filtering, dimensional reduction, and clustering of the data were performed utilizing the SnapATAC2 package in Python (82, 83). Fragment files were imported and processed with sample-specific quality control parameters. Cells were filtered based on the following criteria: minimum fragment counts of 9,000, minimum transcription start site enrichment (TSS enrichment) score of 6, and maximum fragment counts of 90,000 to exclude low-quality nuclei and potential doublets. A tile matrix with 500 bp bins was generated, and the top 250,000 most variable features were selected for downstream analysis. Doublet detection was performed using the Scrublet algorithm implemented in SnapATAC2, and predicted doublets were removed from further analysis.

For dimensional reduction, spectral embedding (similar to Latent Semantic Indexing) was performed on the filtered cells, followed by UMAP for visualization. Cell clustering was performed using the Leiden algorithm after constructing a k-nearest neighbor graph. Cell types were identified by integrating gene activity scores derived from chromatin accessibility profiles with known marker genes and comparison to snRNA-seq data from matched samples.

Statistics

The data were expressed as mean ± standard error of the mean (s.e.m.). Sample sizes for each experiment were specified in the figure legend. Statistical analysis involved conducting one-way or two-way ANOVA followed by the Tukey test for comparing multiple groups, while the unpaired two-tailed Student's t-test was employed for comparing two groups.

Supplementary Figures

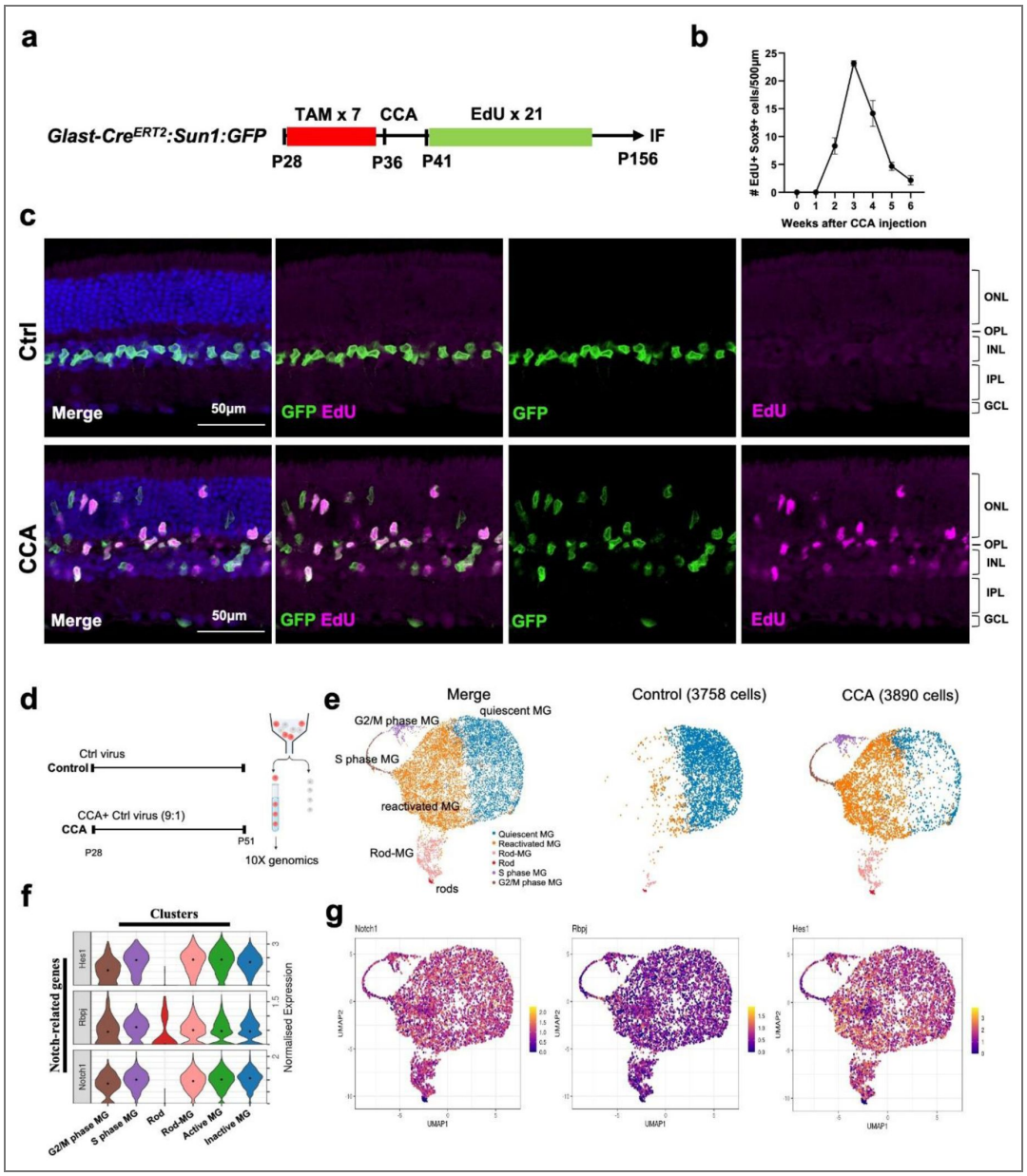

Figure S1. Notch signaling remains active in MG and MG-derived progeny. (a) Schematic illustrating the experimental design for labeling proliferating MG. (b) Schematic illustrating the changes in MG proliferation over time. (c) Representative EdU immunostaining on retinal sections from *Glast-Cre^{ERT2};Sun1:GFP* mice treated with CCA at P28 and collected 4 months post-treatment. (d) Schematic illustration of scRNA-seq experiment. (e) UMAP plot of scRNA-seq data for MG treated with CCA and control virus. (f) Split UMAP plots of the control and CCA groups. (g) Feature plots of normalized Notch related genes, *Notch1*, *Rbpj* and *Hes1* gene expression in different cell clusters.

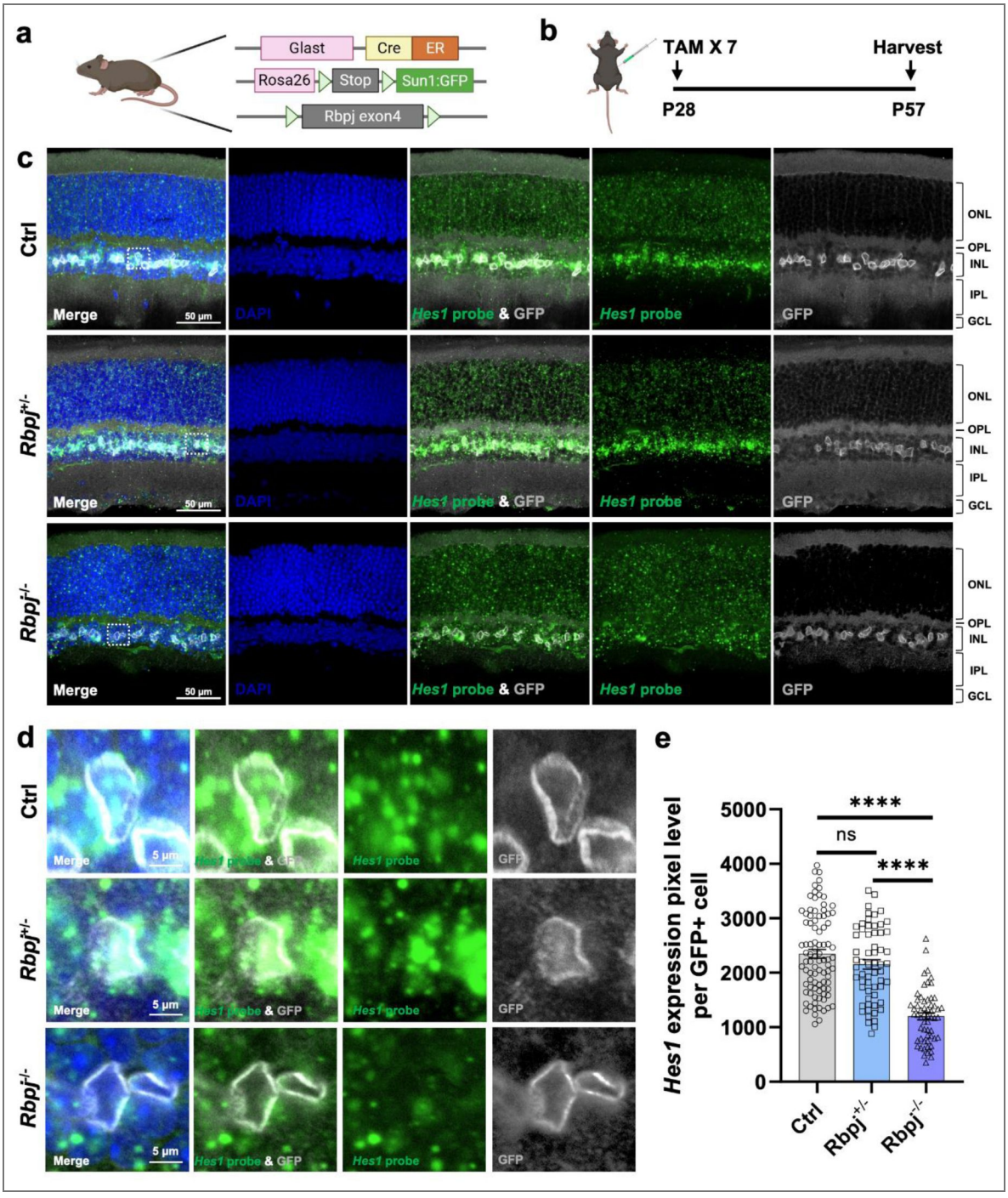

Figure S2. Deletion of *Rbpj* was sufficient to inhibit the canonical Notch signaling pathway.

(a) Schematic of *Glast-Cre*^{ERT2}*;Rbpj*$^{flox/flox}$*;tdT* mouse used in this study. (b) Schematic illustration of the examination of Notch inhibition via *Rbpj* deletion. (c) Hes1 mRNA in situ hybridization in *Glast-Cre*^{ERT2}*;tdT* (Ctrl), *Glast-Cre*^{ERT2}*;Rbpj*$^{flox/wt}$*;tdT* and *Glast-Cre*^{ERT2}*;Rbpj*$^{flox/flox}$*;tdT* mice received tamoxifen (TAM) injection. (d) Magnified views of the highlighted regions in (c). (e) The average pixel level of Hes1 mRNA per GFP+ cell. n≥3 mice, data are presented as mean ± SEM. ns=not significant, ****$P <$ 0.0001, by one-way ANOVA with Tukey's post hoc test.

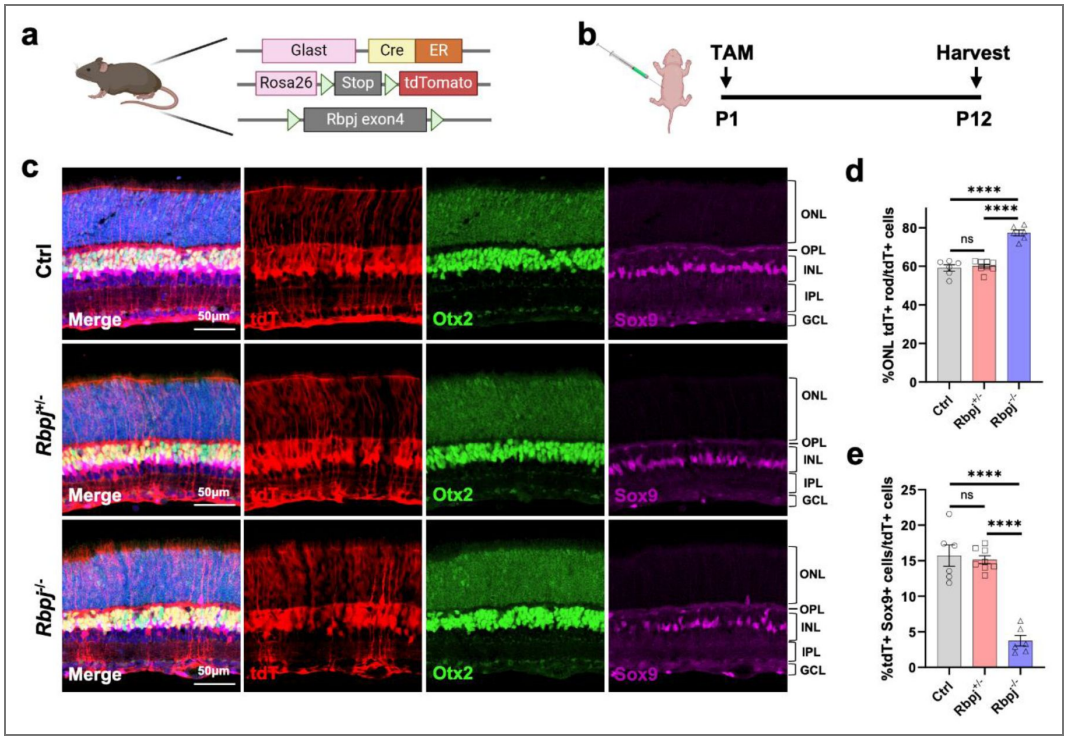

Figure S3. Overproduction of rod photoreceptor cells at expense of MG after Notch signaling inhibition.

(a) Schematic of *Glast-Cre^{ERT2};Rbpj$^{flox/flox}$;Sun1:GFP* mouse used in this study. (b) Schematic illustration of the experiment examining how *Rbpj* deletion affects neurogenesis in retinal progenitor cells. *Glast-Cre^{ERT2};tdT* (Ctrl), *Glast-Cre^{ERT2};Rbpj$^{flox/wt}$;tdT* and *Glast-Cre^{ERT2};Rbpj$^{flox/flox}$;tdT* mice were received TAM injection at postnatal day 1 (P1) and harvested at P12. (c) Representative immunostaining of Otx2 and Sox9 on retinal. (d) Percentage of tdT+ rod photoreceptor cells in overall tdT+ cells. (e) Percentage of tdT+ Sox9+ cells in overall tdT+ cells. n≥3 mice, ns. not significant, ****$P < 0.0001$, by one-way ANOVA with Tukey post hoc test.

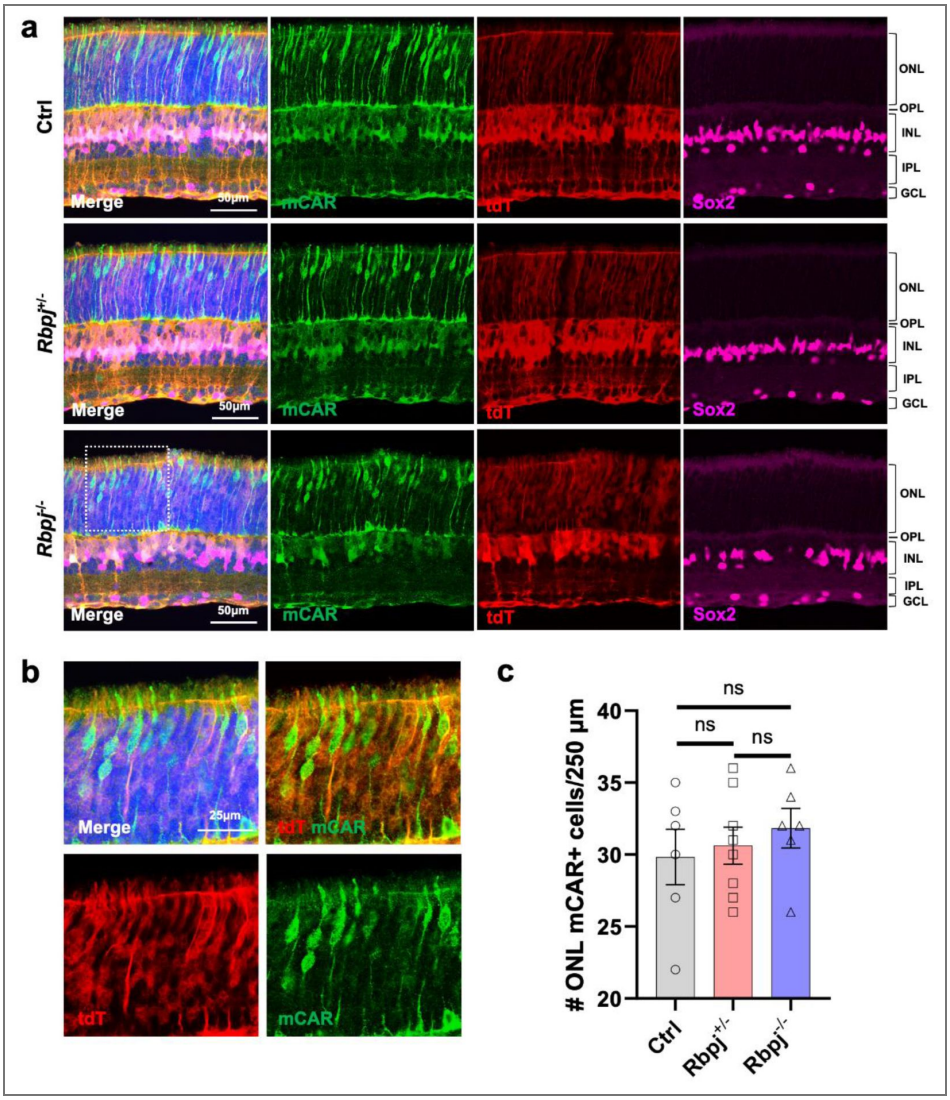

Figure S4. Deletion of *Rbpj* in late RPCs would not affect Cone photoreceptor cells formation.

(a) Representative immunostaining of mCAR and Sox2 on retinal sections from *Glast-Cre^{ERT2};tdT* (Ctrl), *Glast-Cre^{ERT2};Rbpj$^{flox/wt}$;tdT* and *Glast-Cre^{ERT2};Rbpj$^{flox/flox}$;tdT* mice received tamoxifen (TAM) injection at postnatal day 1 (P1) and harvested at P12. (b) Magnified views of the highlighted regions in (a). (c) Number of cone photoreceptor cells in 250μm. n≥3 mice, data are presented as mean ± SEM. ns=not significant, by one-way ANOVA with Tukey's post hoc test.

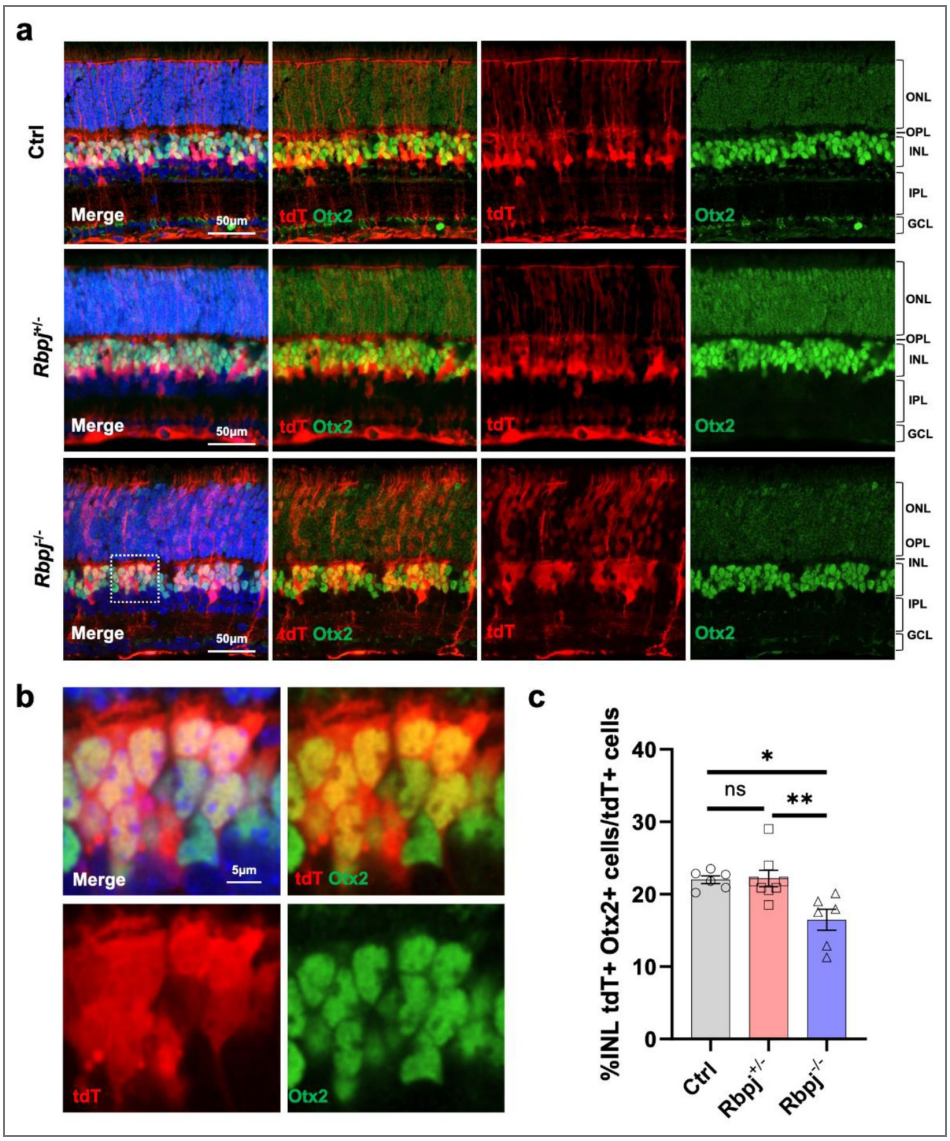

Figure S5. Notch signaling inhibition hindered the BCs generation from late RPCs.

(a) Representative immunostaining of Otx2 on retinal sections from *Glast-Cre^{ERT2};tdT* (Ctrl), *Glast-Cre^{ERT2};Rbpj$^{flox/wt}$;tdT* and *Glast-Cre^{ERT2};Rbpj$^{flox/flox}$;tdT* mice received tamoxifen (TAM) injection at postnatal day 1 (P1) and harvested at P12. (b) Magnified views of the highlighted regions in (a). (c) Percentage of tdT+ Otx2+ cells in overall tdT+ cells. n≥3 mice, ns=not significant, *P < 0.05, **P < 0.01, by one-way ANOVA with Tukey post hoc test.

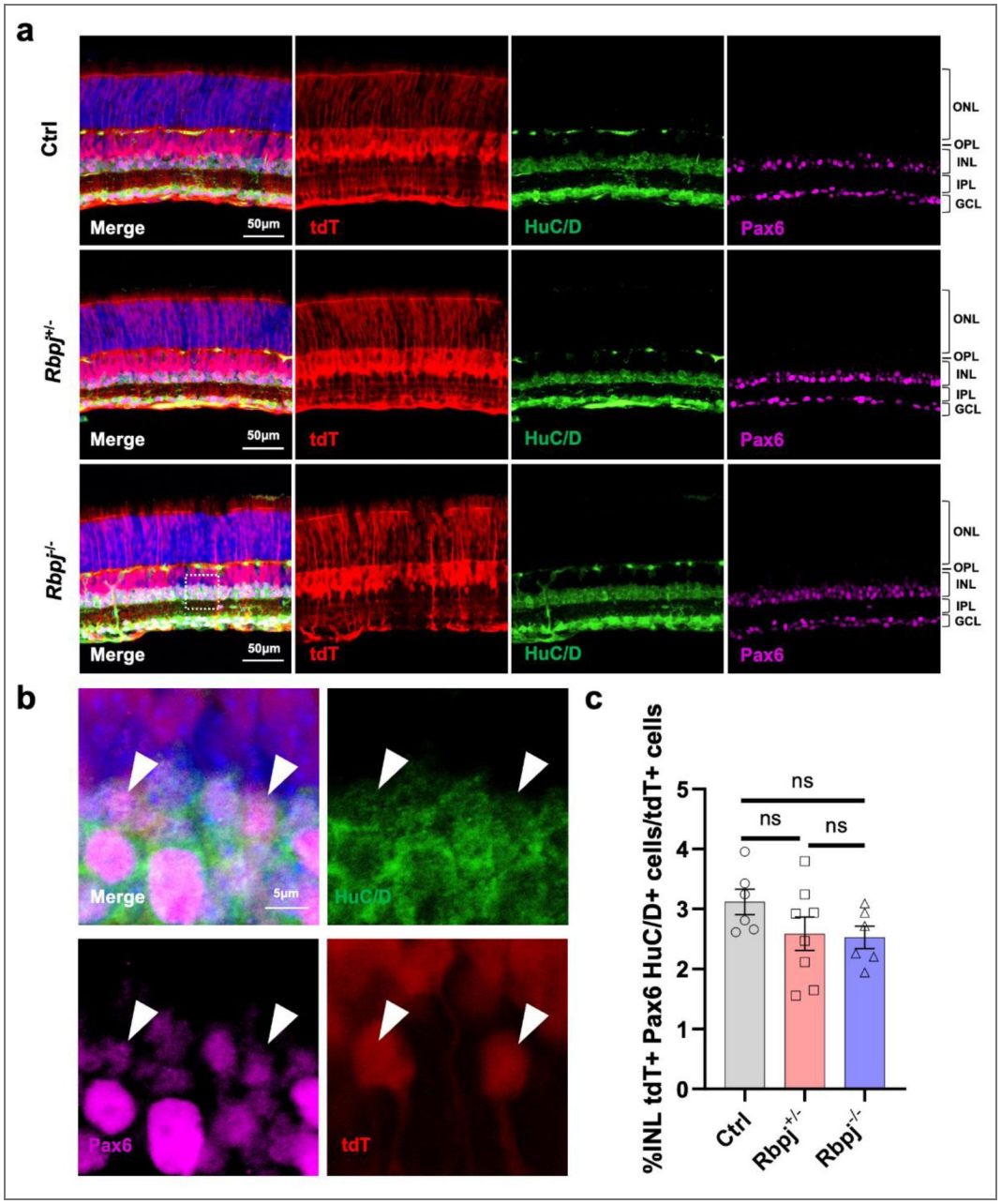

Figure S6. Deletion of *Rbpj* in late RPCs would not affect ACs formation.

(a) Representative immunostaining of HuC/D and Pax6 on retinal sections from *Glast-Cre^{ERT2};tdT* (Ctrl), *Glast-Cre^{ERT2};Rbpj$^{flox/wt}$;tdT* and *Glast-Cre^{ERT2};Rbpj$^{flox/flox}$;tdT* mice received TAM injection at postnatal day 1 (P1) and harvested at P12. (b) Magnified views of the highlighted regions in (a). (c) Percentage of tdT+ HuC/D+ Pax6+ cells in overall tdT+ cells. n≥3 mice, data are presented as mean ± SEM. ns=not significant, by one-way ANOVA with Tukey's post hoc test.

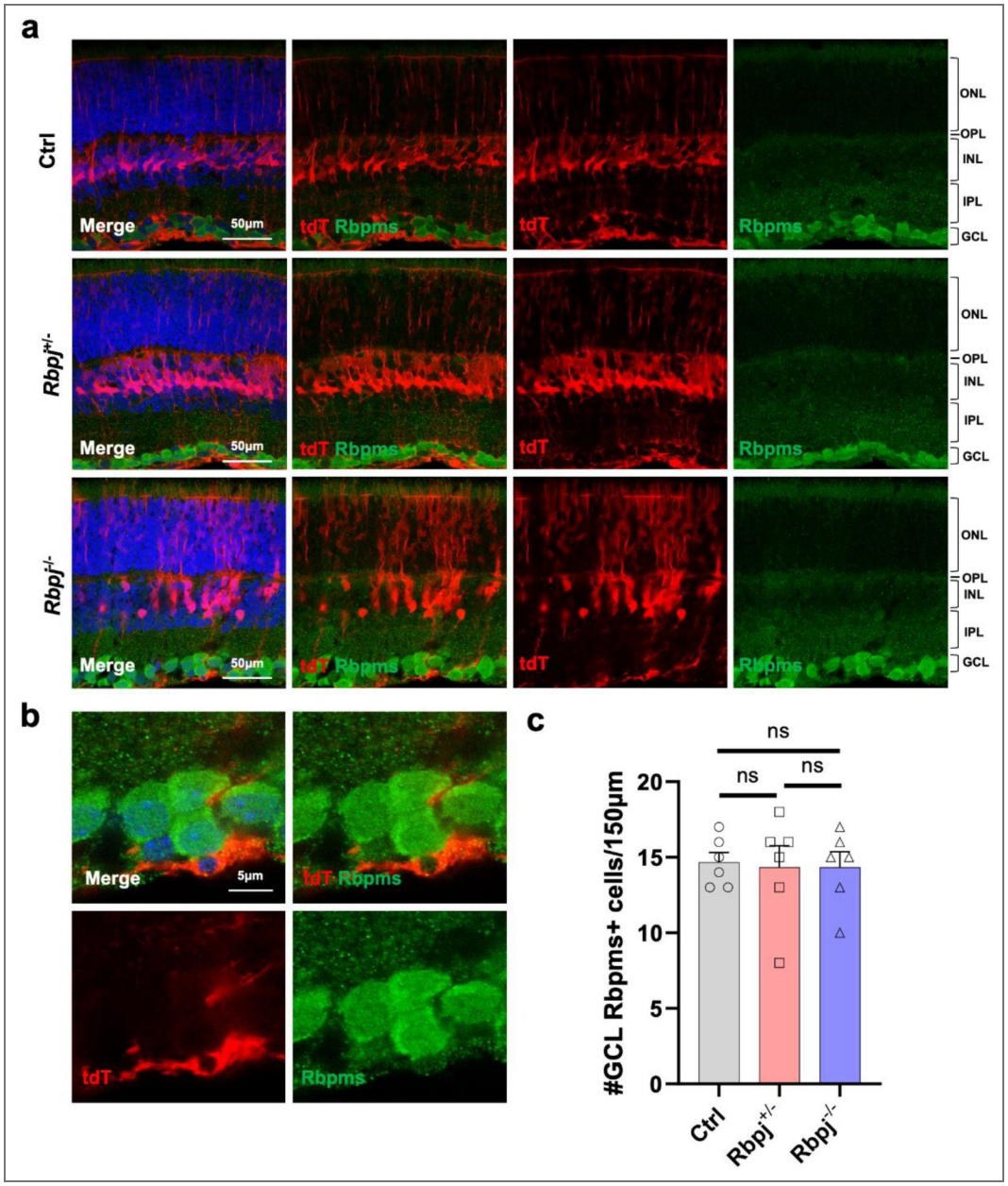

Figure S7. Deletion of *Rbpj* in late RPCs would not affect RGCs formation.

(a) Representative immunostaining of Rbpms on retinal sections from *Glast-Cre^{ERT2};tdT* (Ctrl), *Glast-Cre^{ERT2};Rbpj$^{flox/wt}$;tdT* and *Glast-Cre^{ERT2};Rbpj$^{flox/flox}$;tdT* mice received tamoxifen (TAM) injection at P1 and harvested at P12. (b) Magnified views of the highlighted regions in (a). (c) Number of Rbpms+ cells per 150μm. n≥3 mice, data are presented as mean ± SEM. ns=not significant, by one-way ANOVA with Tukey's post hoc test.

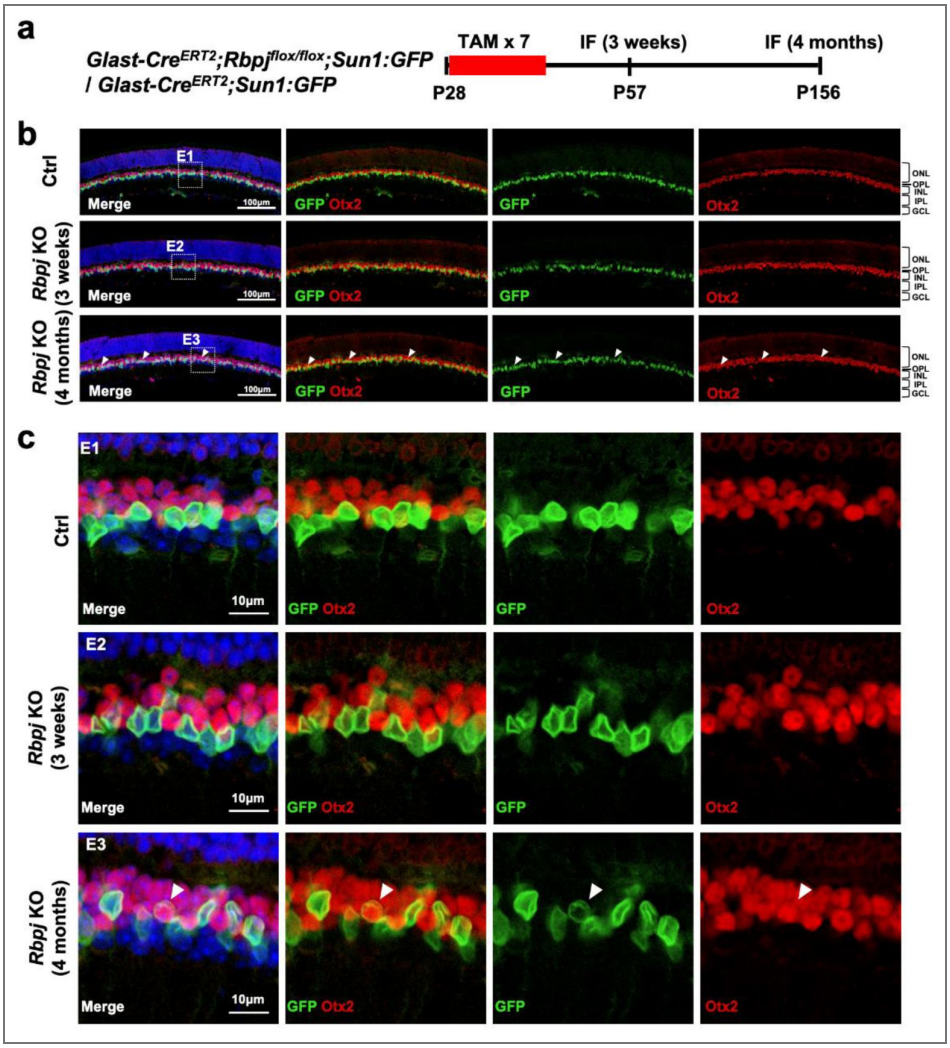

Figure S8. *Rbpj* deletion in adult MG induces limited neuronal conversion.

(a) Schematic illustration of MG dedifferentiation and reprogramming experiment. (b) Representative immunostaining of Sox9 on retinal sections from *Glast-Cre^{ERT2};Sun1:GFP* and *Glast-Cre^{ERT2};Rbpj$^{flox/flox}$;Sun1:GFP* mice harvested at different timepoints post TAM injection. The white arrows refer to GFP+ Sox9- cells. (c) Magnified views of the highlighted regions in (B).

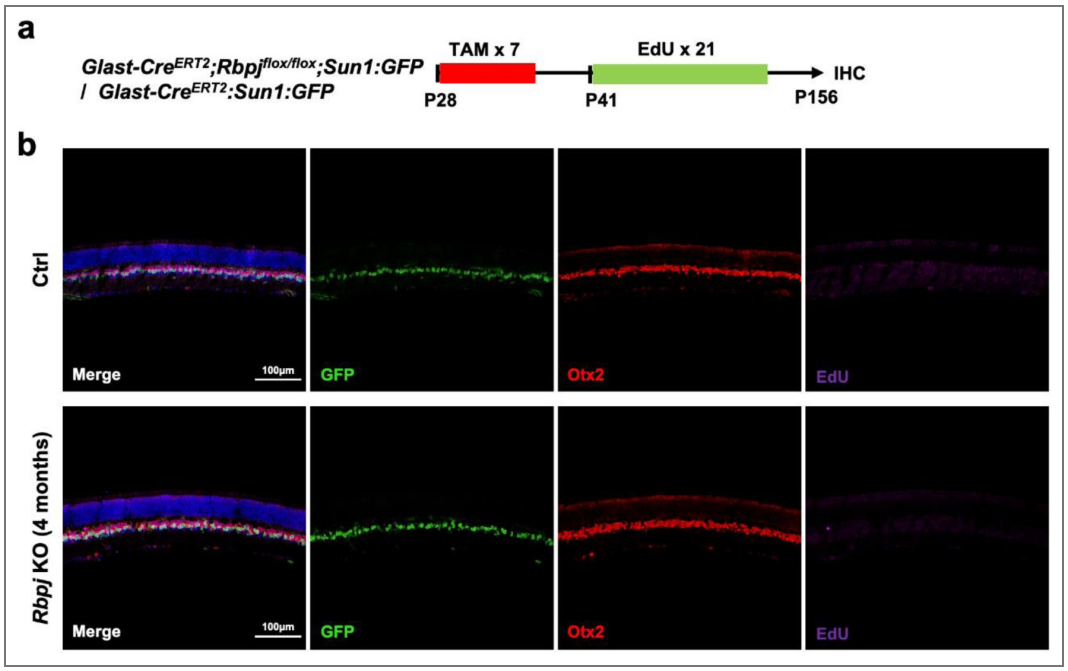

Figure S9. *Rbpj* deletion induces transdifferentiation-mediated neurogenesis in adult MG.

(a) Schematic illustration of the experiment examining MG proliferation. (b) Representative immunostaining of Otx2 and EdU on retinal sections from *Glast-Cre^{ERT2};Sun1:GFP* and *Glast-Cre^{ERT2};Rbpj$^{flox/flox}$;Sun1:GFP* mice harvested at 4 months post TAM injection.

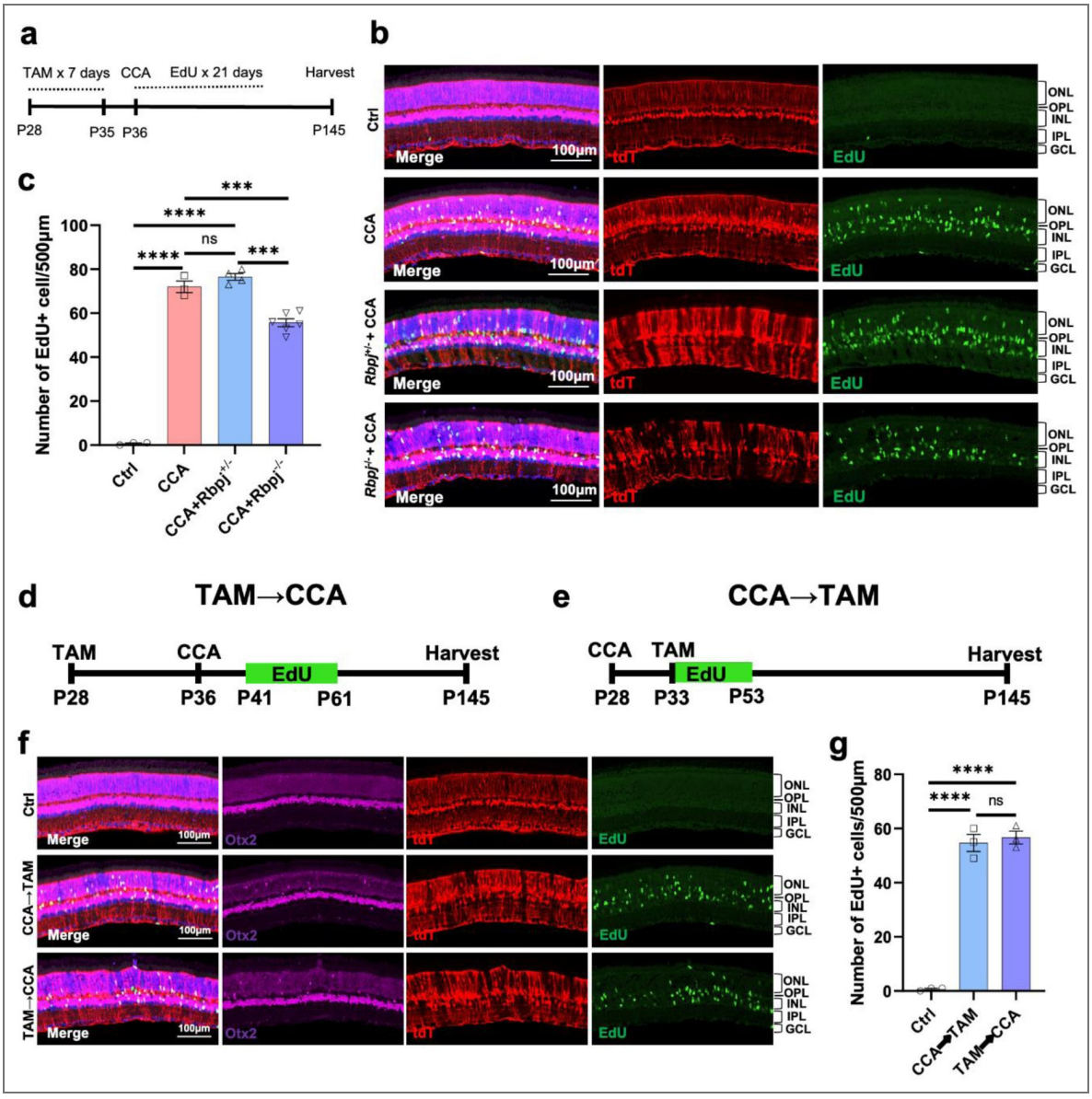

Figure S10. Notch inhibition reduced MG proliferation induced by CCA, yet it did not entirely prevent it.

(a) Schematic illustration of proliferation level comparison experiment. (b) Representative immunostaining of EdU on retinal sections from *Glast-Cre^{ERT2};tdT* (Ctrl), *Glast-Cre^{ERT2};Rbpj$^{flox/wt}$;tdT* and *Glast-Cre^{ERT2};Rbpj$^{flox/flox}$;tdT* mice received CCA injection. (c) Number of EdU+ cells in 500μm. n≥3 mice, data are presented as mean ± SEM. ns=not significant, ***$P < 0.001$; ****$P < 0.0001$, by one-way ANOVA with Tukey's post hoc test. (d-e) Schematic illustration of the comparison of proliferation levels between different CCA injection and TAM administration orders. (f) Representative immunostaining of EdU on retinal sections from *Glast-Cre^{ERT2};Rbpj$^{flox/flox}$;tdT* mice received CCA injection. (g) Number of EdU+ cells in 500μm. n=3 mice, data are presented as mean ± SEM. ns=not significant, ****$P < 0.0001$, by one-way ANOVA with Tukey's post hoc test.

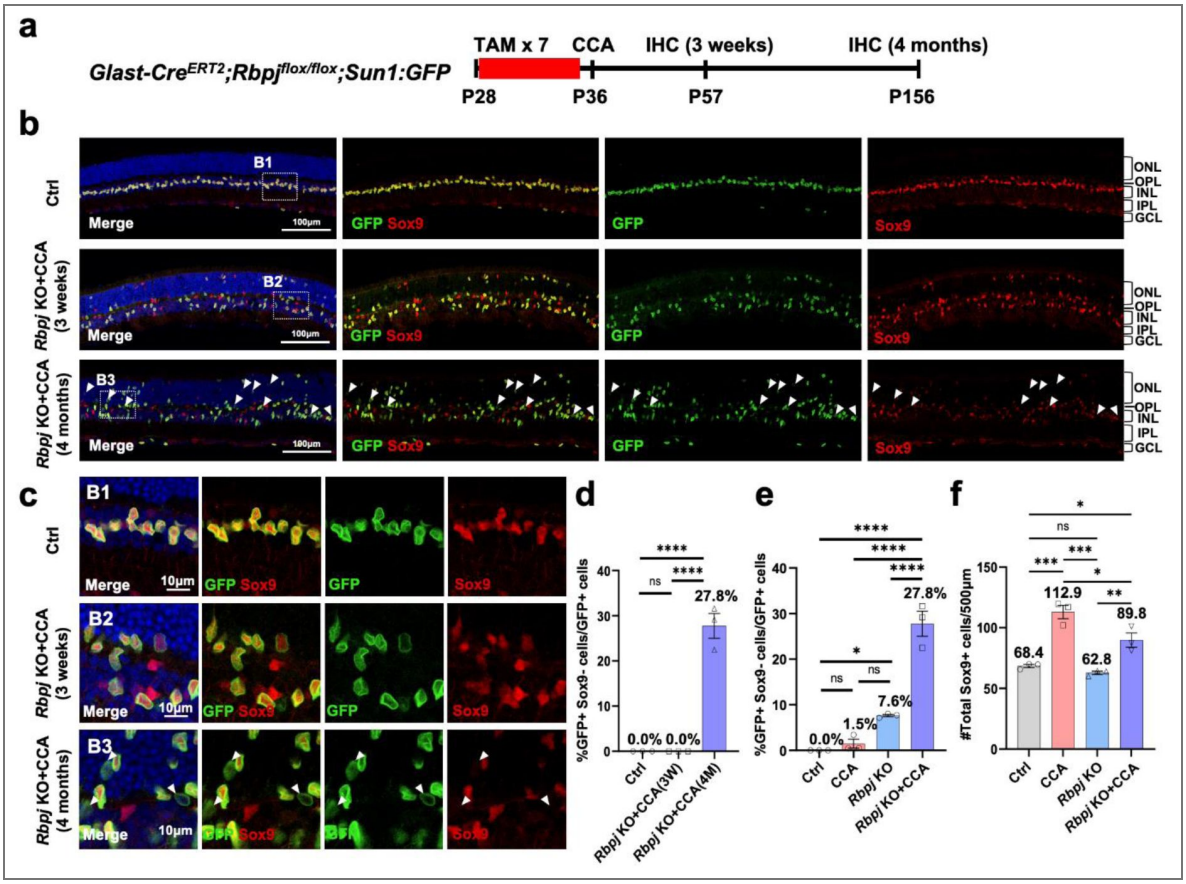

Figure S11. The synergistic effect of *Rbpj* KO and CCA resulted in a robust MG dedifferentiation.

(a) Schematic illustration of MG dedifferentiation experiment. (b) Representative immunostaining of Sox9 on retinal sections from *Glast-Cre^{ERT2};Sun1:GFP* (Ctrl) and *Glast-Cre^{ERT2};Rbpj$^{flox/flox}$;Sun1:GFP* mice at 3 weeks and 4 months post CCA treatment. The white arrows refer to GFP+ Sox9- cells. (c) Magnified views of the highlighted regions in (b). (d) Percentage of GFP+ Sox9- cells in overall GFP+ cells. 3W: 3 weeks, 4M: 4 months, n=3 mice, data are presented as mean ± SEM. ns=not significant, ****P < 0.0001, by one-way ANOVA with Tukey's post hoc test. (e) Percentage of GFP$^+$ Sox9$^-$ cells among total GFP$^+$ cells in the 4-month samples. n=3 mice, data are presented as mean ± SEM. ns=not significant, *P < 0.05, ****P < 0.0001, by one-way ANOVA with Tukey's post hoc test. (f) Number of Sox9+ cells per 500μm in the 4-month samples. n=3 mice, data are presented as mean ± SEM. ns=not significant, *P < 0.05, **P < 0.01, ***P < 0.001, by one-way ANOVA with Tukey's post hoc test.

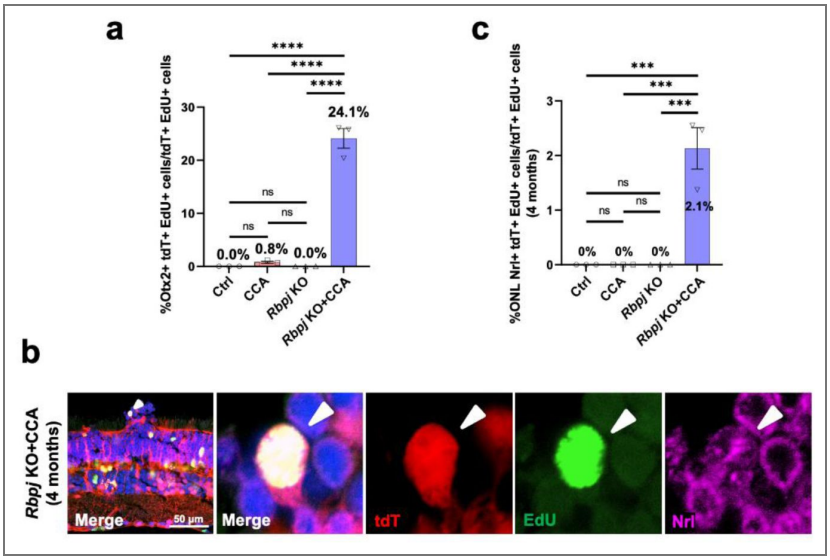

Figure S12. The synergistic effect of *Rbpj* KO and CCA resulted in a robust MG reprogramming.

(a) Percentage of tdT+ EdU+ Otx2+ cells in overall tdT+ EdU+ cells. n=3 mice, data are presented as mean ± SEM. ns=not significant, ****$P < 0.0001$, by one-way ANOVA with Tukey's post hoc test. (b) Representative immunostaining of EdU and Nrl on retinal sections. (c) Percentage of tdT+ EdU+ Nrl+ cells in ONL tdT+ EdU+ cells. n=3 mice, data are presented as mean ± SEM. ns=not significant, ***$P < 0.001$, by one-way ANOVA with Tukey's post hoc test.

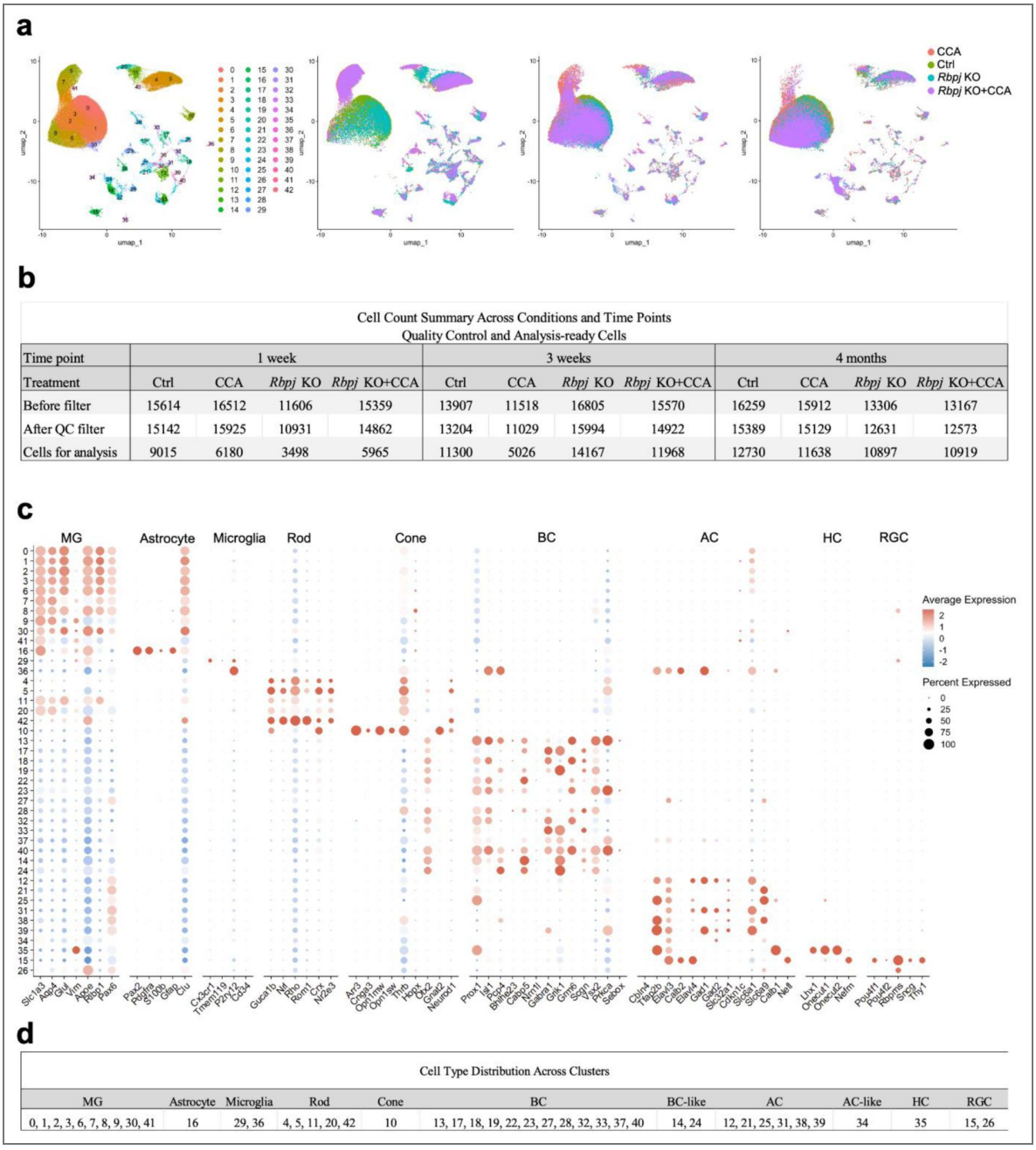

b

Cell Count Summary Across Conditions and Time Points
Quality Control and Analysis-ready Cells

Time point	1 week				3 weeks				4 months			
Treatment	Ctrl	CCA	*Rbpj* KO	*Rbpj* KO+CCA	Ctrl	CCA	*Rbpj* KO	*Rbpj* KO+CCA	Ctrl	CCA	*Rbpj* KO	*Rbpj* KO+CCA
Before filter	15614	16512	11606	15359	13907	11518	16805	15570	16259	15912	13306	13167
After QC filter	15142	15925	10931	14862	13204	11029	15994	14922	15389	15129	12631	12573
Cells for analysis	9015	6180	3498	5965	11300	5026	14167	11968	12730	11638	10897	10919

d

Cell Type Distribution Across Clusters

MG	Astrocyte	Microglia	Rod	Cone	BC	BC-like	AC	AC-like	HC	RGC
0, 1, 2, 3, 6, 7, 8, 9, 30, 41	16	29, 36	4, 5, 11, 20, 42	10	13, 17, 18, 19, 22, 23, 27, 28, 32, 33, 37, 40	14, 24	12, 21, 25, 31, 38, 39	34	35	15, 26

Figure S13. Preprocessing and filtering of snRNA data.

(a) The UMAP before the removal of contamination cells. The original mature neurons affecting the analysis were removal. (b) Number of cells passing quality control and used for snRNA-seq analysis. (c) Dot plot showing the expression of marker genes of each cluster in unfiltered UMAP. (d) The initial annotation of clusters in the unfiltered UMAP.

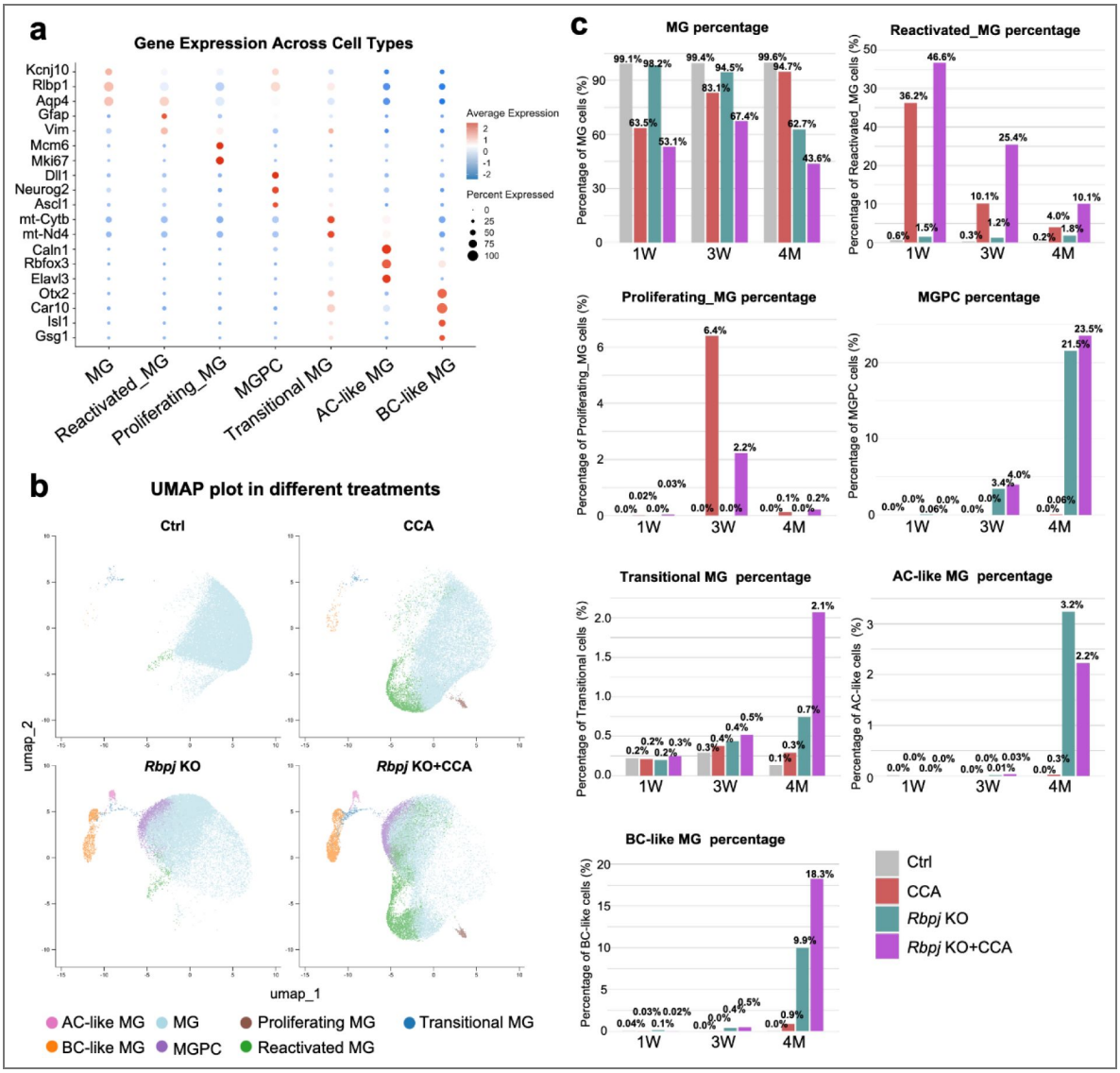

Figure S14. Additional snRNA-seq analysis of MG at 1 week, 3 weeks and 4 months post-CCA treatment.

(a) Dot plot showing gene expression and cell percentages for quiescent MG, proliferating MG, reactivated MG, MGPC, transitional MG, AC-like MG, BC-like MG. (b) Separated UMAP plot of snRNA-seq data of Ctrl, CCA, *Rbpj* KO, *Rbpj* KO+CCA treatment. (c) Separated proportions of cell clusters within Ctrl, CCA, *Rbpj* KO and *Rbpj* KO+CCA groups at different timepoints.

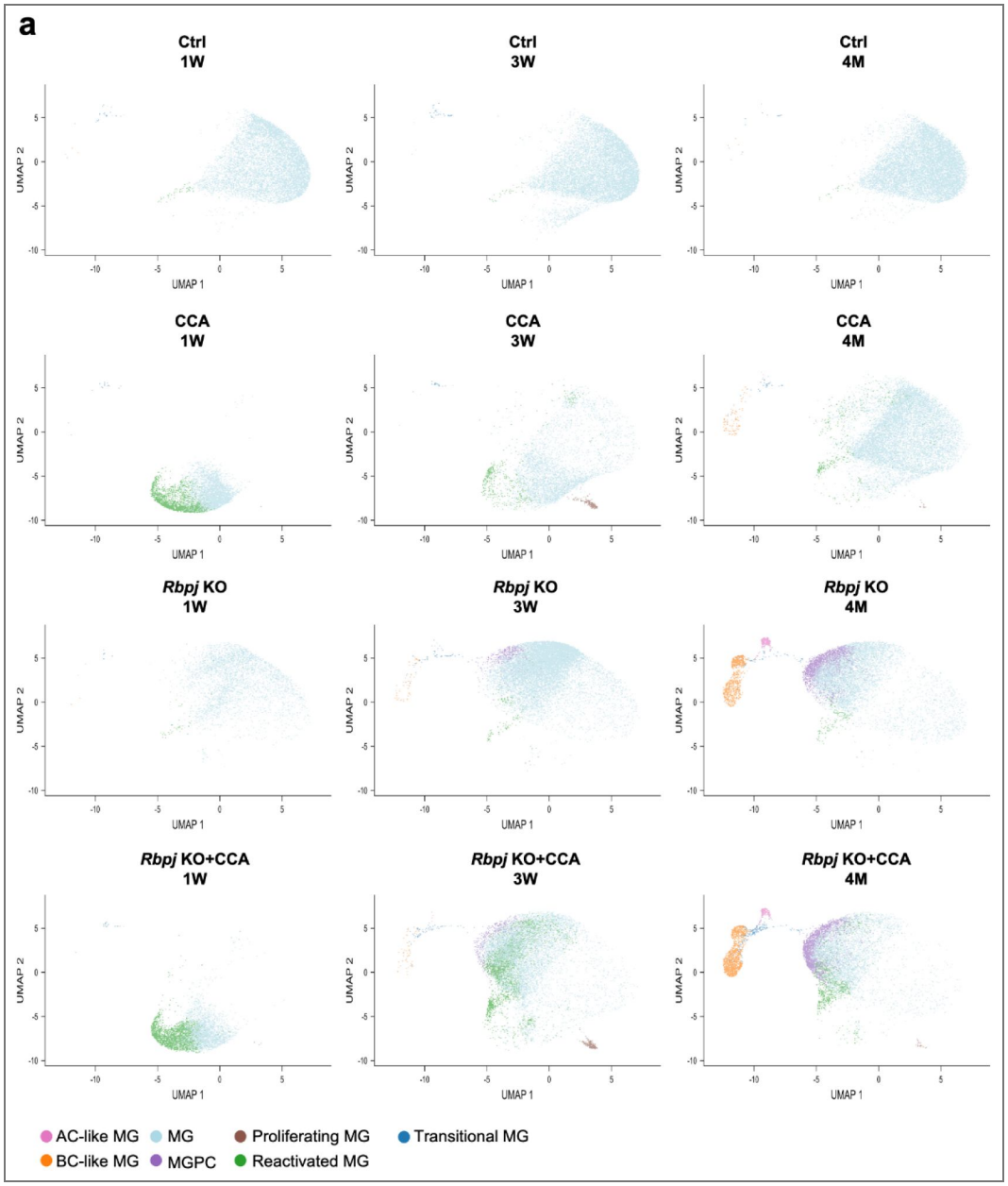

Figure S15. Separation of UMAP by different timepoints and treatments.

(a) The split UMAP by the condition of time and treatment. To monitor the progress of MG regeneration, we implemented three time points (1 week (1W), 3 weeks (3W), 4 months (4M)) and four treatment groups (Ctrl, CCA, *Rbpj* KO, *Rbpj* KO+CCA).

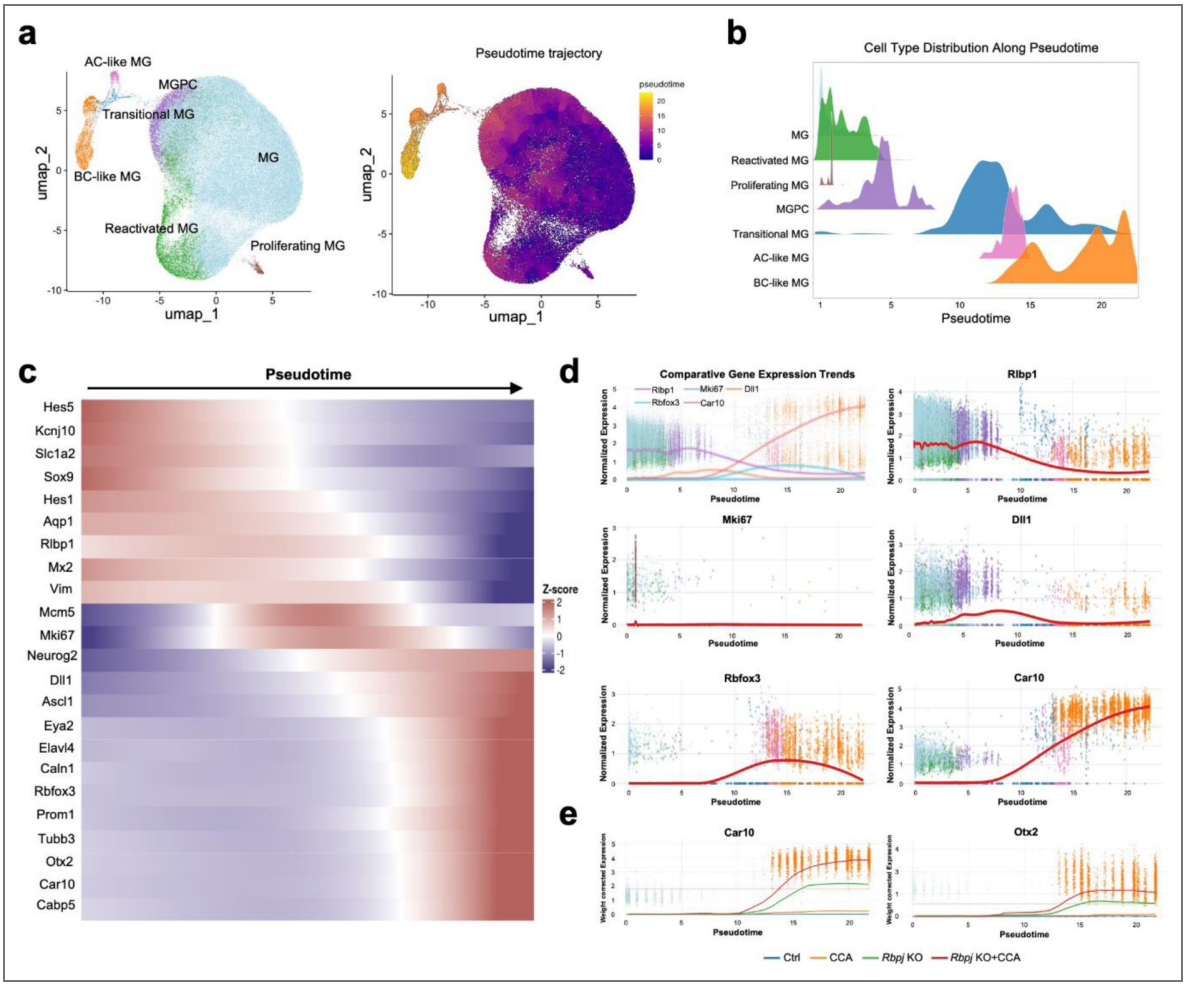

Figure S16. Pseudotime trajectory analysis of MG reprogramming process.

(a) Pseudotime trajectory analysis showing the MG reprogramming process. (b) Dynamic cell type distribution along the pseudotime. (c) Change of gene expression level along the pseudotime. MG (Hes5, Kcnj10, Slc1a2, Sox9, Hes1, Aqp1, Rlbp1); Reactivated MG (Mx2, Vim); Proliferating MG (Mcm5, Mki67); MGPC (Neurog2, Dll1, Ascl1, Eya2); AC-like (Elavl4, Caln1, Rbfox3); photoreceptor cell (Prom1); RGC (Tubb3); BC-like (Otx2, Car10, Cabp5). (d) Gene expression trends along pseudotime. (e) Separated gene expression trends along pseudotime.

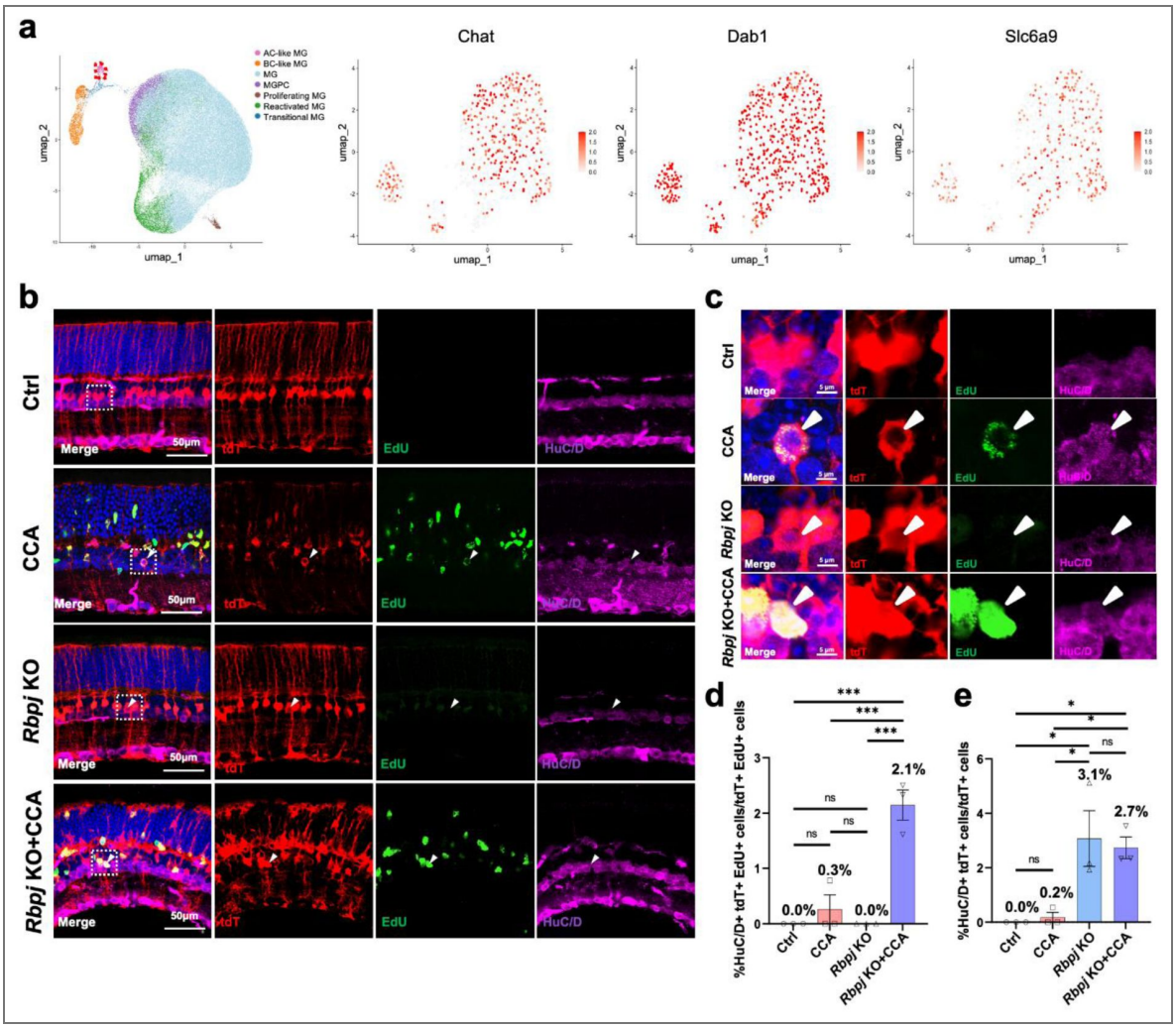

Figure S17. Subclustering analysis of the AC-like population.

(a) Feature plots of AC-like subtypes showing the expression patterns of Chat (starburst ACs), Dab1 (A17 ACs), and Slc6a9 (nGnG ACs). The AC-like population is outlined in red. (b) Representative immunostaining of EdU and HuC/D on retinal sections. The white arrows refer to tdT+ HuC/D+ cells. (c) Magnified views of the highlighted regions in (b). (d) Percentage of tdT+ EdU+ HuC/D+ cells in overall tdT+ EdU+ cells. n=3 mice, data are presented as mean ± SEM. ns=not significant, ***P < 0.001, by one-way ANOVA with Tukey's post hoc test. (e) Percentage of tdT+ HuC/D+ cells in overall tdT+ cells. n=3 mice, data are presented as mean ± SEM. ns=not significant, *P < 0.05, by one-way ANOVA with Tukey's post hoc test.

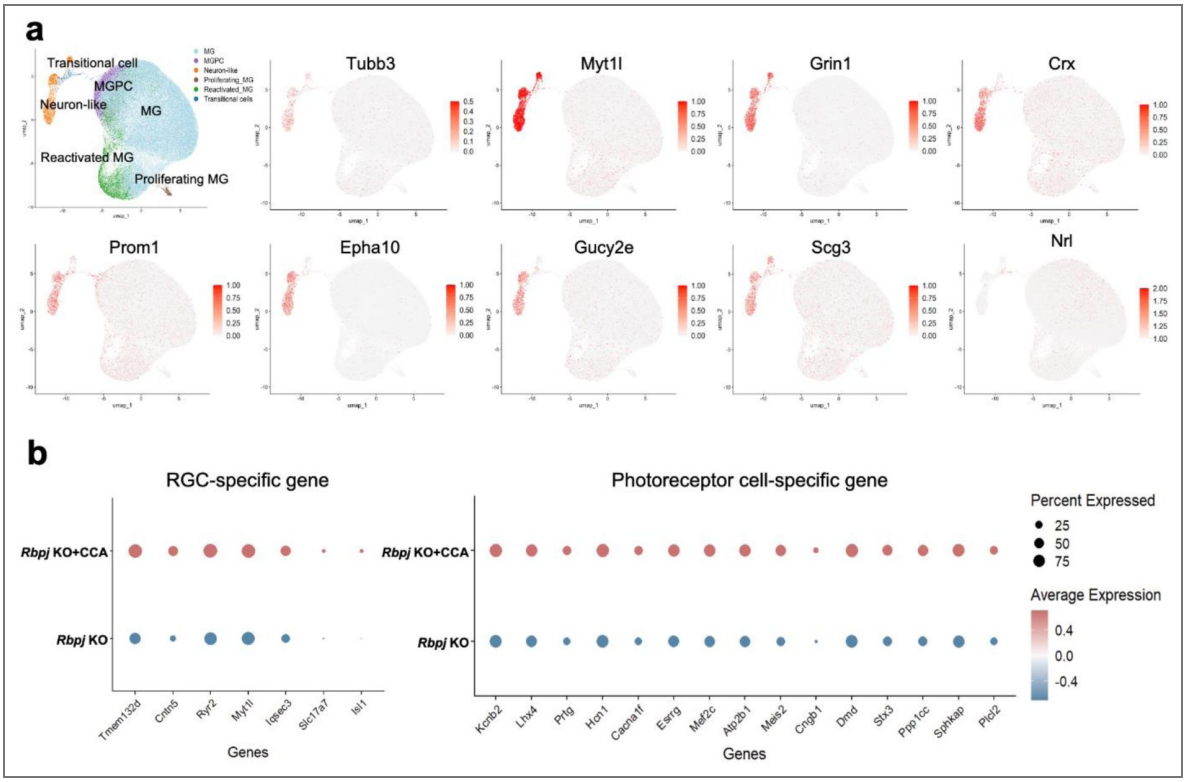

Figure S18. The newborn neurons showed diverse gene expression profiles linked to different neuronal cell types.

(a) Feature plots showing the additional neuronal markers related to RGC and photoreceptor cells. (b) Dot plots showing different expression of RGC-specific and photoreceptor cells-specific genes ($p<0.05$).

Figure S19. Preprocessing and filtering of snATAC data.

(a) The UMAP before the removal of contamination cells. (b) Dot plot showing the expression of marker genes of each cluster in unfiltered UMAP. (c) The initial annotation of clusters in the unfiltered UMAP.

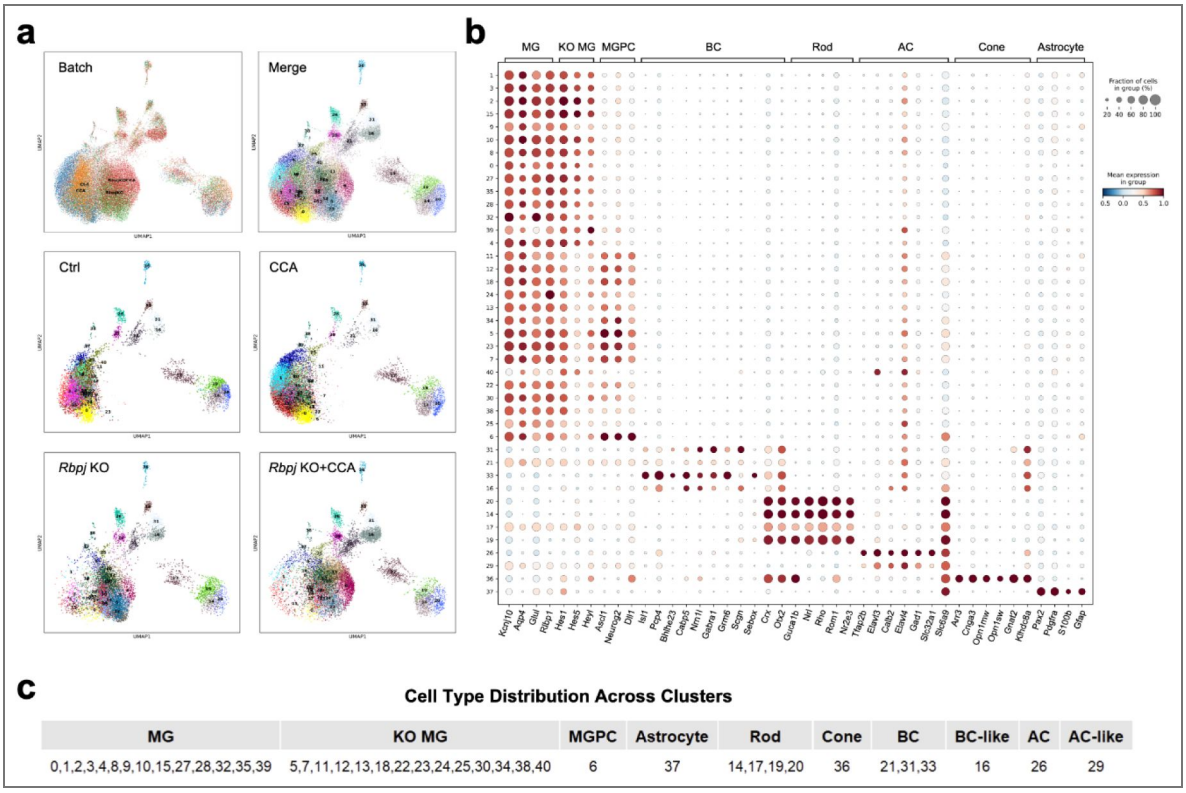

c

Cell Type Distribution Across Clusters

MG	KO MG	MGPC	Astrocyte	Rod	Cone	BC	BC-like	AC	AC-like
0,1,2,3,4,8,9,10,15,27,28,32,35,39	5,7,11,12,13,18,22,23,24,25,30,34,38,40	6	37	14,17,19,20	36	21,31,33	16	26	29

Figure S20. Expression pattern of ZO1 in the retina.

(a) Schematic illustration of ZO1 staining experiment. (b) Representative immunostaining of Otx2 and ZO1 on retinal sections from *Glast-Cre^{ERT2};tdT* and *Glast-Cre^{ERT2};Rbpj$^{flox/flox}$;tdT* mice at 9 months post TAM injection. The white arrows refer to tdT+ Otx2+ cells.

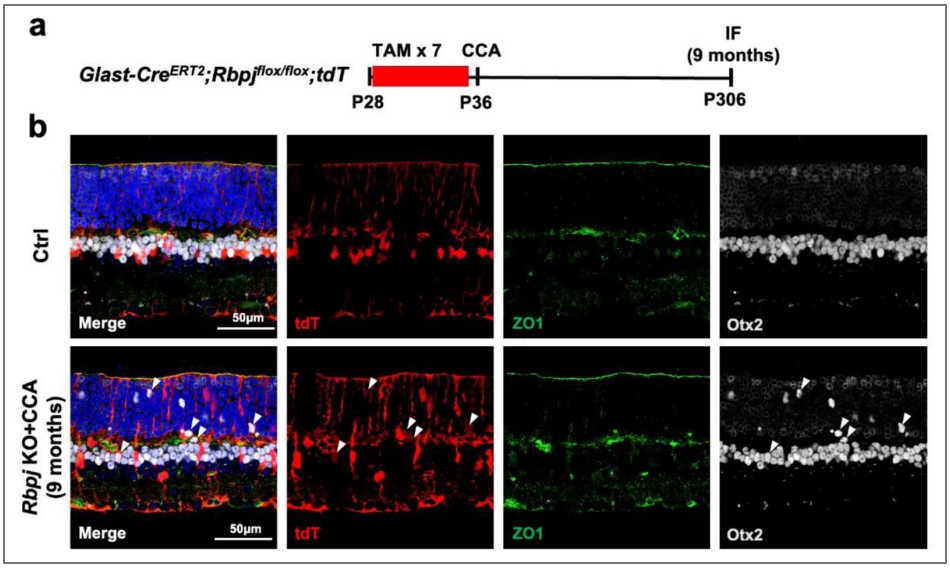

Data availability

The RNA sequence data used in this study will be made publicly available in GEO upon completion of the peer-review process.

Acknowledgements

This research was funded by Research Grants Council Hong Kong Project (11103819, 11102922, and 11100723), Hong Kong Health and Medical Research Fund Project (05160276 and 06172466), TUNG Biomedical Sciences Foundation, and Ming Wai Lau Center for Reparative Medicine Research Associate Program.

Additional information

Author contributions

W.X. and B.L. conceived and designed the project. B.L. performed the experiments, collected and analyzed the data. B.L., Y.J., and S.L. carried out cell sorting and prepared the snRNA-seq and snATAC-seq libraries. L.C. and C.L. processed the Chromium Next GEM single-nucleus data using Cell Ranger. B.L. analyzed the snRNA-seq and snATAC-seq datasets, with assistance from C.L., B.L., W.W., H.T., and J.X. handled mouse work. B.L., J.Z. and Q.Z. optimized RNAscope imaging. B.L. wrote the original draft and organized the figures. W.X. reviewed and edited the manuscript and acquired funding.

Funding

Funder	Grant reference number	Author
Research Grants Council, University Grants Committee (研究資助局)	11103819	Wenjun Xiong
Research Grants Council, University Grants Committee (研究資助局)	11102922	Wenjun Xiong
Research Grants Council, University Grants Committee (研究資助局)	11100723	Wenjun Xiong
Hong Kong Health and Medicial Research Fund Project	05160276	Wenjun Xiong
Hong Kong Health and Medicial Research Fund Project	06172466	Wenjun Xiong

Author ORCID iDs

Lingxi Chen: https://orcid.org/0000-0002-5229-7470
Qinrong Zhang: https://orcid.org/0000-0001-8893-514X
Wenjun Xiong: https://orcid.org/0000-0001-6836-2807

References

1. **Roesch K.,** Stadler M. B., Cepko C. L. (2012) Gene expression changes within Müller glial cells in retinitis pigmentosa. *Mol Vis* **18**:1197-1214 PubMed
2. **Jadhav A. P.,** Roesch K., Cepko C. L. (2009) Development and neurogenic potential of Müller glial cells in the vertebrate retina. *Prog Retin Eye Res* **28**:249-262 https://doi.org/10.1016/j.preteyeres.2009.05.002 | PubMed
3. **Cepko C. L.,** Austin C. P., Yang X., Alexiades M., Ezzeddine D. (1996) Cell fate determination in the vertebrate retina. *Proceedings of the National Academy of Sciences* **93**:589-595 https://doi.org/10.1073/pnas.93.2.589 | PubMed

4. **Todd L.,** Reh T. A. (2022) Comparative Biology of Vertebrate Retinal Regeneration: Restoration of Vision through Cellular Reprogramming. *Cold Spring Harb Perspect Biol* **14** https://doi.org/10.1101/cshperspect.a040816 | PubMed
5. **Lahne M.,** Nagashima M., Hyde D. R., Hitchcock P. F. (2020) Reprogramming Müller Glia to Regenerate Retinal Neurons. *Annu Rev Vis Sci* 171-193 https://doi.org/10.1146/annurev-vision-121219-081808 | PubMed
6. **Wan J.,** Goldman D. (2016) Retina regeneration in zebrafish. *Current Opinion in Genetics & Development* https://doi.org/10.1016/j.gde.2016.05.009 | PubMed
7. **Fischer A. J.** (2005) Neural regeneration in the chick retina. *Prog Retin Eye Res* **24**:161-182 https://doi.org/10.1016/j.preteyeres.2004.07.003 | PubMed
8. **Fischer A. J.,** Reh T. A. (2001) Müller glia are a potential source of neural regeneration in the postnatal chicken retina. *Nat Neurosci* 247-252 https://doi.org/10.1038/85090 | PubMed
9. **Bringmann A.,** Iandiev I., Pannicke T., Wurm A., Hollborn M., Wiedemann P., Osborne N. N., Reichenbach A. (2009) Cellular signaling and factors involved in Müller cell gliosis: Neuroprotective and detrimental effects. *Prog Retin Eye Res* **28**:423-451 https://doi.org/10.1016/j.preteyeres.2009.07.001 | PubMed
10. **Wu Z.,** Liao B., Ying J., Keung J., Zheng Z., Ahola V., Xiong W. (2025) Simultaneous cyclin D1 overexpression and p27kip1 knockdown enable robust Müller glia cell cycle reactivation in uninjured mouse retina. *eLife* 1-31 https://doi.org/10.7554/elife.100904 | PubMed
11. **Yao K.,** Qiu S., Tian L., Snider W. D., Flannery J. G., Schaffer D. V., Chen B. (2016) Wnt Regulates Proliferation and Neurogenic Potential of Müller Glial Cells via a Lin28/let-7 miRNA-Dependent Pathway in Adult Mammalian Retinas. *Cell Rep* **17**:165-178 https://doi.org/10.1016/j.celrep.2016.08.078 | PubMed
12. **Rueda E. M.,** Hall B. M., Hill M. C., Swinton P. G., Tong X., Martin J. F., Poche R. A. (2019) The Hippo Pathway Blocks Mammalian Retinal Müller Glial Cell Reprogramming. *Cell Rep* 1637-1649 https://doi.org/10.1016/j.celrep.2019.04.047 | PubMed
13. **Hamon A.,** García-García D., Ail D., Bitard J., Chesneau A., Dalkara D., Locker M., Roger J. E., Perron M. (2019) Linking YAP to Müller Glia Quiescence Exit in the Degenerative Retina. *Cell Rep* **27**:1712-1725.e6 https://doi.org/10.1016/j.celrep.2019.04.045 | PubMed
14. **Mills E. A.,** Goldman D. (2017) The Regulation of Notch Signaling in Retinal Development and Regeneration. *Curr Pathobiol Rep* **176**:100-106 https://doi.org/10.1007/s40139-017-0153-7 | PubMed
15. **Shimojo H.,** Ohtsuka T., Kageyama R. (2008) Oscillations in Notch Signaling Regulate Maintenance of Neural Progenitors. *Neuron* **58**:52-64 https://doi.org/10.1016/j.neuron.2008.02.014 | PubMed
16. **Conner C.,** Ackerman K. M., Lahne M., Hobgood J. S., Hyde D. R. (2014) Repressing notch signaling and expressing TNFα are sufficient to mimic retinal regeneration by inducing müller glial proliferation to generate committed progenitor cells. *Journal of Neuroscience* **34**:14403-14419 https://doi.org/10.1523/jneurosci.0498-14.2014 | PubMed
17. **Goldman D.** (2014) Müller glial cell reprogramming and retina regeneration. *Nat Rev Neurosci* **15**:431-442 https://doi.org/10.1038/nrn3723 | PubMed
18. **Campbell L. J.,** Hobgood J. S., Jia M., Boyd P., Hipp R. I., Hyde D. R. (2021) Notch3 and DeltaB maintain Müller glia quiescence and act as negative regulators of regeneration in the light-damaged zebrafish retina. *Glia* **69**:546-566 https://doi.org/10.1002/glia.23912 | PubMed
19. **Elsaeidi F.,** Macpherson P., Mills E. A., Jui J., Flannery J. G., Goldman D. (2018) Notch suppression collaborates with Ascl1 and Lin28 to unleash a regenerative response in fish retina, but not in mice. *Journal of Neuroscience* **38**:2246-2261 https://doi.org/10.1523/jneurosci.2126-17.2018 | PubMed
20. **Li X.-J.,** Morgan C., Li L., Zhang W.-Y., Chrysostomou E., Doetzlhofer A. (2025) The Notch ligand Jagged1 plays a dual role in cochlear hair cell regeneration. *Nat Commun* **16**:8169 https://doi.org/10.1038/s41467-025-63053-6 | PubMed

21. **Shu Y.,** Li W., Huang M., Quan Y. Z., Scheffer D., Tian C., Tao Y., Liu X., Hochedlinger K., Indzhykulian A. A., *et al.* (2019) Renewed proliferation in adult mouse cochlea and regeneration of hair cells. *Nat Commun* **10**:1-15 https://doi.org/10.1038/s41467-019-13157-7 | PubMed

22. **Zamboni M.,** Llorens-Bobadilla E., Magnusson J. P., Frisén J. (2020) A Widespread Neurogenic Potential of Neocortical Astrocytes Is Induced by Injury. *Cell Stem Cell* **27**:605-617.e5 https://doi.org/10.1016/j.stem.2020.07.006 | PubMed

23. **Magnusson J. P.,** Göritz C., Tatarishvili J., Dias D. O., Smith E. M. K., Lindvall O., Kokaia Z., Frisén J. (2014) A latent neurogenic program in astrocytes regulated by Notch signaling in the mouse. *Science (1979)* **346**:237-241 https://doi.org/10.1126/science.346.6206.237 | PubMed

24. **Le N.,** Awad S., Palazzo I., Hoang T., Blackshaw S. (2025) Viral-mediated Oct4 overexpression and inhibition of Notch signaling synergistically induce neurogenic competence in mammalian Müller glia. *eLife* 1-33 https://doi.org/10.7554/elife.106450.2

25. **Le N.,** Vu T. D., Palazzo I., Pulya R., Kim Y., Blackshaw S., Hoang T. (2024) Robust reprogramming of glia into neurons by inhibition of Notch signaling and nuclear factor I (NFI) factors in adult mammalian retina. *Sci Adv* **10**:1-16 https://doi.org/10.1126/sciadv.adn2091 | PubMed

26. **Campbell L. J.,** Levendusky J. L., Steines S. A., Hyde D. R. (2022) Retinal regeneration requires dynamic Notch signaling. *Neural Regen Res* **17**:1199-1209 https://doi.org/10.4103/1673-5374.327326 | PubMed

27. **Borggrefe T.,** Oswald F. (2009) The Notch signaling pathway: Transcriptional regulation at Notch target genes. *Cellular and Molecular Life Sciences* **66**:1631-1646 https://doi.org/10.1007/s00018-009-8668-7 | PubMed

28. **Yoon K.,** Gaiano N. (2005) Notch signaling in the mammalian central nervous system: Insights from mouse mutants. *Nat Neurosci* **8**:709-715 https://doi.org/10.1038/nn1475 | PubMed

29. **Trimarchi J. M.,** Stadler M. B., Cepko C. L. (2008) Individual retinal progenitor cells display extensive heterogeneity of gene expression. *PLoS One* **3** https://doi.org/10.1371/journal.pone.0001588 | PubMed

30. **Nelson B. R.,** Ueki Y., Reardon S., Karl M. O., Georgi S., Hartman B. H., Lamba D. A., Reh T. A. (2011) Genome-wide analysis of Müller glial differentiation reveals a requirement for notch signaling in postmitotic cells to maintain the glial fate. *PLoS One* **6** https://doi.org/10.1371/journal.pone.0022817 | PubMed

31. **Jadhav A. P.,** Mason H. A., Cepko C. L. (2006) Notch 1 inhibits photoreceptor production in the developing mammalian retina. *Development* 913-923 https://doi.org/10.1242/dev.02245 | PubMed

32. **Yaron O.,** Farhy C., Marquardt T., Applebury M., Ashery-Padan R. (2006) Notch1 functions to suppress cone-photoreceptor fate specification in the developing mouse retina. *Development* **133**:1367-1378 https://doi.org/10.1242/dev.02311 | PubMed

33. **Jadhav A. P.,** Cho S. H., Cepko C. L. (2006) Notch activity permits retinal cells to progress through multiple progenitor states and acquire a stem cell property. *Proc Natl Acad Sci U S A* **103**:18998-19003 https://doi.org/10.1073/pnas.0608155103 | PubMed

34. **Rowan S.,** Conley K. W., Le T. T., Donner A. L., Maas R. L., Brown N. L. (2008) Notch signaling regulates growth and differentiation in the mammalian lens. *Dev Biol* **321**:111-122 https://doi.org/10.1016/j.ydbio.2008.06.002 | PubMed

35. **Molday R. S.,** Moritz O. L. (2015) Photoreceptors at a glance. *J Cell Sci* **128**:4039-4045 https://doi.org/10.1242/jcs.175687 | PubMed

36. **Hartong D.,** Berson E., Dryja T. (2006) Retinitis pigmentosa Prevalence and inheritance patterns. *Lancet* **368**:1795-1809 https://doi.org/10.1016/s0140-6736(06)69740-7 | PubMed

37. **Mears A. J.,** Kondo M., Swain P. K., Takada Y., Bush R. A., Saunders T. L., Sieving P. A., Swaroop A. (2001) Nrl is required for rod photoreceptor development. *Nat Genet* **29**:447-452 https://doi.org/10.1038/ng774 | PubMed

38. **Leino S. A.,** Constable S. C. J., Streit A., Wilkinson D. G. (2023) Zbtb16 mediates a switch between Fgf signalling regimes in the developing hindbrain. *Development* **150** https://doi.org/10.1242/dev.201319 | PubMed

39. **Oproescu A. M.,** Han S., Schuurmans C. (2021) New Insights Into the Intricacies of Proneural Gene Regulation in the Embryonic and Adult Cerebral Cortex. *Frontiers in Molecular Neuroscience* https://doi.org/10.3389/fnmol.2021.642016 | PubMed

40. **Henke R. M.,** Savage T. K., Meredith D. M., Glasgow S. M., Hori K., Dumas J., MacDonald R. J., Johnson J. E. (2009) Neurog2 is a direct downstream target of the Ptf1a-Rbpj transcription complex in dorsal spinal cord. *Development* **136**:2945-2954 https://doi.org/10.1242/dev.035352 | PubMed

41. **Nelson C. M.,** Gorsuch R. A., Bailey T. J., Ackerman K. M., Kassen S. C., Hyde D. R. (2012) Stat3 defines three populations of müller glia and is required for initiating maximal müller glia proliferation in the regenerating zebrafish retina. *Journal of Comparative Neurology* **520**:4294-4311 https://doi.org/10.1002/cne.23213 | PubMed

42. **Todd L.,** Squires N., Suarez L., Fischer A. J. (2016) Jak/Stat signaling regulates the proliferation and neurogenic potential of Müller glia-derived progenitor cells in the avian retina. *Sci Rep* **6**:1-16 https://doi.org/10.1038/srep35703 | PubMed

43. **Jorstad N. L.,** Wilken M. S., Todd L., Finkbeiner C., Nakamura P., Radulovich N., Hooper M. J., Chitsazan A., Wilkerson B. A., Rieke F., *et al.* (2020) STAT Signaling Modifies Ascl1 Chromatin Binding and Limits Neural Regeneration from Muller Glia in Adult Mouse Retina. *Cell Rep* **30**:2195-2208.e5 https://doi.org/10.1016/j.celrep.2020.01.075 | PubMed

44. **Minegishi Y.,** Iejima D., Kobayashi H., Chi Z. L., Kawase K., Yamamoto T., Seki T., Yuasa S., Fukuda K., Iwata T. (2013) Enhancedoptineurin E50k-TBK1 interaction evokes protein insolubility and initiates familial primary open-angle glaucoma. *Hum Mol Genet* **22**:3559-3567 https://doi.org/10.1093/hmg/ddt210 | PubMed

45. **Hoang T.,** Wang J., Boyd P., Wang F., Santiago C., Jiang L., Yoo S., Lahne M., Todd L. J., Jia M., *et al.* (2020) Gene regulatory networks controlling vertebrate retinal regeneration. *Science (1979)* **8598**:eabb8598 https://doi.org/10.1126/science.abb8598 | PubMed

46. **Prieto-López L.,** Pereiro X., Vecino E. (2024) The mechanics of the retina: Müller glia role on retinal extracellular matrix and modelling. *Frontiers in Medicine* https://doi.org/10.3389/fmed.2024.1393057 | PubMed

47. **Shekhar K.,** Lapan S. W., Whitney I. E., Tran N. M., Macosko E. Z., Kowalczyk M., Adiconis X., Levin J. Z., Nemesh J., Goldman M., *et al.* (2016) Comprehensive Classification of Retinal Bipolar Neurons by Single-Cell Transcriptomics. *Cell* **166**:1308-1323.e30 https://doi.org/10.1016/j.cell.2016.07.054 | PubMed

48. **Yan W.,** Laboulaye M. A., Tran N. M., Whitney I. E., Benhar I., Sanes J. R. (2020) Mouse Retinal Cell Atlas: Molecular Identification of over Sixty Amacrine Cell Types. *Journal of Neuroscience* **40**:5177-5195 https://doi.org/10.1523/jneurosci.0471-20.2020 | PubMed

49. **Monroe T. O.,** Hill M. C., Morikawa Y., Leach J. P., Heallen T., Cao S., Krijger P. H. L., de Laat W., Wehrens X. H. T., Rodney G. G., *et al.* (2019) YAP Partially Reprograms Chromatin Accessibility to Directly Induce Adult Cardiogenesis In Vivo. *Dev Cell* **48**:765-779.e7 https://doi.org/10.1016/j.devcel.2019.01.017 | PubMed

50. **Papp B.,** Plath K. (2013) Epigenetics of reprogramming to induced pluripotency. *Cell* https://doi.org/10.1016/j.cell.2013.02.043 | PubMed

51. **Reichenbach A.,** Bringmann A. (2013) New functions of müller cells. *Glia* **61**:651-678 https://doi.org/10.1002/glia.22477 | PubMed

52. **Bringmann A.,** Pannicke T., Grosche J., Francke M., Wiedemann P., Skatchkov S. N., Osborne N. N., Reichenbach A. (2006) Müller cells in the healthy and diseased retina. *Prog Retin Eye Res* **25**:397-424 https://doi.org/10.1016/j.preteyeres.2006.05.003 | PubMed

53. **Lenkowski J. R.,** Raymond P. A. (2014) Müller glia: Stem cells for generation and regeneration of retinal neurons in teleost fish. *Prog Retin Eye Res* **40**:94-123 https://doi.org/10.1016/j.preteyeres.2013.12.007 | PubMed

54. **Gorsuch R. A.,** Hyde D. R. (2014) Regulation of Müller glial dependent neuronal regeneration in the damaged adult zebrafish retina. *Exp Eye Res* **123**:131-140 https://doi.org/10.1016/j.exer.2013.07.012 | PubMed

55. **Noctor Stephen C.,** Flint Alexander C., Weissman Tamily A., Dammerman Ryan S., Kriegstein Arnold R. (2001) Neurons derived from radial glial cells establish radial units in neocortex. *Nature* 714-720 https://doi.org/10.1038/35055553 | PubMed

56. **McMahon S. S.,** McDermott K. W. (2006) A comparison of cell transplantation and retroviral gene transfection as tools to study lineage and differentiation in the rat spinal cord. *J Neurosci Methods* **152**:243-249 https://doi.org/10.1016/j.jneumeth.2005.09.008 | PubMed

57. **Ruiz S.,** Panopoulos A. D., Herrerías A., Bissig K. D., Lutz M., Berggren W. T., Verma I. M., Izpisua Belmonte J. C. (2011) A high proliferation rate is required for cell reprogramming and maintenance of human embryonic stem cell identity. *Current Biology* **21**:45-52 https://doi.org/10.1016/j.cub.2010.11.049 | PubMed

58. **Hanna J.,** Saha K., Pando B., Van Zon J., Lengner C. J., Creyghton M. P., Van Oudenaarden A., Jaenisch R. (2009) Direct cell reprogramming is a stochastic process amenable to acceleration. *Nature* **462**:595-601 https://doi.org/10.1038/nature08592 | PubMed

59. **Wolffe A. P.** (1991) Implications of DNA replication for eukaryotic gene expression. *J Cell Sci* **99**:201-206 https://doi.org/10.1242/jcs.99.2.201 | PubMed

60. **Yeo R. W.,** Zhou O. Y., Zhong B. L., Sun E. D., Navarro Negredo P., Nair S., Sharmin M., Ruetz T. J., Wilson M., Kundaje A., *et al.* (2023) Chromatin accessibility dynamics of neurogenic niche cells reveal defects in neural stem cell adhesion and migration during aging. *Nat Aging* **3**:866-893 https://doi.org/10.1038/s43587-023-00449-3 | PubMed

61. **Li M.,** Guo H., Carey M., Huang C. (2024) Transcriptional and epigenetic dysregulation impairs generation of proliferative neural stem and progenitor cells during brain aging. *Nat Aging* **4**:62-79 https://doi.org/10.1038/s43587-023-00549-0 | PubMed

62. **Gómez-Gaviro M. V.,** Scott C. E., Sesay A. K., Matheu A., Booth S., Galichet C., Lovell-Badge R. (2012) Betacellulin promotes cell proliferation in the neural stem cell niche and stimulates neurogenesis. *Proc Natl Acad Sci U S A* **109**:1317-1322 https://doi.org/10.1073/pnas.1016199109 | PubMed

63. **Riesenberg A. N.,** Liu Z., Kopan R., Brown N. L. (2009) Rbpj Cell Autonomous Regulation of Retinal Ganglion Cell and Cone Photoreceptor Fates in the Mouse Retina. *The Journal of Neuroscience* **29**:12865-12877 https://doi.org/10.1523/jneurosci.3382-09.2009 | PubMed

64. **Furukawa Takahisa,** Mukherjee Siddhartha, Bao Zheng-Zheng, Morrow Eric M. (2000) Constance L. Cepko, rax, Hes1, and notch1 Promote the Formation of Müller Glia by Postnatal Retinal Progenitor Cells. *Neuron* **26**:383-394 https://doi.org/10.1016/s0896-6273(00)81171-x | PubMed

65. **Fogerty J.,** Song P., Boyd P., Grabinski S. E., Hoang T., Reich A., Cianciolo L. T., Blackshaw S., Mumm J. S., Hyde D. R., *et al.* (2022) Notch Inhibition Promotes Regeneration and Immunosuppression Supports Cone Survival in a Zebrafish Model of Inherited Retinal Dystrophy. *Journal of Neuroscience* **42**:5144-5158 https://doi.org/10.1523/jneurosci.0244-22.2022 | PubMed

66. **Sahu A.,** Devi S., Jui J., Goldman D. (2021) Notch signaling via Hey1 and Id2b regulates Müller glia's regenerative response to retinal injury. *Glia* **69**:2882-2898 https://doi.org/10.1002/glia.24075 | PubMed

67. **Hayes S.,** Nelson B. R., Buckingham B., Reh T. A. (2007) Notch signaling regulates regeneration in the avian retina. *Dev Biol* 300-311 https://doi.org/10.1016/j.ydbio.2007.09.046 | PubMed

68. **Kimura A.,** Namekata K., Guo X., Harada C., Harada T. (2016) Neuroprotection, growth factors and BDNF-TRKB signalling in retinal degeneration. *International Journal of Molecular Sciences* https://doi.org/10.3390/ijms17091584

69. **Kolomeyer A. M.,** Zarbin M. A. (2014) Trophic factors in the pathogenesis and therapy for retinal degenerative diseases. *Survey of Ophthalmmology* https://doi.org/10.1016/j.survophthal.2013.09.004 | PubMed

70. **Ahmed M.,** Kojima Y., Masai I. (2022) Strip1 regulates retinal ganglion cell survival by suppressing Jun-mediated apoptosis to promote retinal neural circuit formation. *eLife* **11**:1-34 https://doi.org/10.7554/elife.74650 | PubMed

71. **Oswald J.,** Kegeles E., Minelli T., Volchkov P., Baranov P. (2021) Transplantation of miPSC/mESC-derived retinal ganglion cells into healthy and glaucomatous retinas. *Mol Ther Methods Clin Dev* **21**:180-198 https://doi.org/10.1016/j.omtm.2021.03.004 | PubMed

72. **Soucy J. R.,** Todd L., Kriukov E., Phay M., Malechka V. V., Rivera J. D., Reh T. A., Baranov P. (2017) Controlling donor and newborn neuron migration and maturation in the eye through microenvironment engineering. *Proceedings of the National Academy of Sciences* **120**:2017 https://doi.org/10.1073/pnas.2302089120 | PubMed

73. **Zadro Lamoureux L. A.,** Zacks D. N., Baker A. N., Zheng Q. D., Hauswirth W. W., Tsilfidis C. (2009) Effects on XIAP retinal detachment-induced photoreceptor apoptosis. *Invest Ophthalmol Vis Sci* **50**:1448-1453 https://doi.org/10.1167/iovs.08-2855 | PubMed

74. **Donovan M.,** Doonan F., Cotter T. G. (2006) Decreased expression of pro-apoptotic Bcl-2 family members during retinal development and differential sensitivity to cell death. *Dev Biol* **291**:154-169 https://doi.org/10.1016/j.ydbio.2005.12.026 | PubMed

75. **Dent E. W.,** Barnes A. M., Tang F., Kalil K. (2004) Netrin-1 and Semaphorin 3A Promote or Inhibit Cortical Axon Branching, Respectively, by Reorganization of the Cytoskeleton. *Journal of Neuroscience* **24**:3002-3012 https://doi.org/10.1523/jneurosci.4963-03.2004 | PubMed

76. **Alto L. T.,** Terman J. R. (2017) Semaphorins and their signaling mechanisms. *Methods in Molecular Biology* **1493**:1-25 https://doi.org/10.1007/978-1-4939-6448-2_1 | PubMed

77. **Madisen L.,** Zwingman T. A., Sunkin S. M., Oh S. W., Zariwala H. A., Gu H., Ng L. L., Palmiter R. D., Hawrylycz M. J., Jones A. R., *et al.* (2010) A robust and high-throughput Cre reporting and characterization system for the whole mouse brain. *Nat Neurosci* **13**:133-140 https://doi.org/10.1038/nn.2467 | PubMed

78. **Mo A.,** Mukamel E. A., Davis F. P., Luo C., Henry G. L., Picard S., Urich M. A., Nery J. R., Sejnowski T. J., Lister R., *et al.* (2015) Epigenomic Signatures of Neuronal Diversity in the Mammalian Brain. *Neuron* **86**:1369-1384 https://doi.org/10.1016/j.neuron.2015.05.018 | PubMed

79. **Wang Y.,** Rattner A., Zhou Y., Williams J., Smallwood P. M., Nathans J. (2012) Norrin/Frizzled4 signaling in retinal vascular development and blood brain barrier plasticity. *Cell* **151**:1332-1344 https://doi.org/10.1016/j.cell.2012.10.042 | PubMed

80. **Hoang D. A.,** Liao B., Zheng Z., Xiong W. (2023) Mutation-independent gene knock-in therapy targeting 5'UTR for autosomal dominant retinitis pigmentosa. *Signal Transduct Target Ther* **8** https://doi.org/10.1038/s41392-022-01308-0 | PubMed

81. **Stuart T.,** Butler A., Hoffman P., Hafemeister C., Papalexi E., Mauck W. M., Hao Y., Stoeckius M., Smibert P., Satija R. (2019) Comprehensive Integration of Single-Cell Data. *Cell* **177**:1888-1902.e21 https://doi.org/10.1016/j.cell.2019.05.031 | PubMed

82. **Fang R.,** Preissl S., Li Y., Hou X., Lucero J., Wang X., Motamedi A., Shiau A. K., Zhou X., Xie F., *et al.* (2021) Comprehensive analysis of single cell ATAC-seq data with SnapATAC. *Nat Commun* **12** https://doi.org/10.1038/s41467-021-21583-9 | PubMed

83. **Zhang K.,** Zemke N. R., Armand E. J., Ren B. (2024) A fast, scalable and versatile tool for analysis of single-cell omics data. *Nat Methods* **21**:217-227 https://doi.org/10.1038/s41592-023-02139-9 | PubMed

Wenjun Xiong (2026) Synergistic Inhibition of Notch Signaling and Forced Cell Cycle Re-entry Drive Müller Glia Reprogramming in Uninjured Mouse Retina. Dryad Digital Repository. https://doi.org/10.5061/dryad.573n5tbpr

Peer reviews

Reviewer #1 (Public review):

Summary:

This study examines Müller glia (MG) reprogramming in the uninjured mouse retina through a combination of Notch signaling inhibition and AAV-induced proliferation. Building on their prior work showing that Cyclin D1 overexpression and p27^Kip1^ knockdown (CCA) promotes MG proliferation with very limited neurogenesis, the authors now demonstrate that Rbpj deletion alone induces a modest degree of MG-to-neuron conversion without proliferation, in agreement with recent work in the field. However, combining Rbpj deletion with CCA-mediated proliferation substantially enhances MG dedifferentiation and the generation of retinal neuron-like cells. Through genetic lineage tracing, histological analyses, and single-cell transcriptomics, the authors provide evidence that MG-derived cells acquire molecular features of bipolar (ON, OFF, and rod bipolar) and amacrine neurons. Most MG-derived cells appear to survive long-term (up to 9 months).

Strengths:

Overall, the study is carefully designed and executed, and the manuscript is clearly written with well-presented figures. While the work does not significantly expand the repertoire of neuronal types generated from mammalian MG beyond what has been previously reported in the field, it provides a valuable and improved strategy for inducing robust MG proliferation and neurogenesis in the mammalian retina.

Weaknesses:

(1) It would be better to include a negative control AAV when evaluating the effect of CCA AAV in the Rbpj KO background. This could help distinguish the specific contribution of the CCA construct from potential effects of intravitreal AAV injection itself, which can induce mild inflammation, known to influence MG reprogramming.

(2) The extent of MG transduction by the CCA AAV is not clear. As quantifications are normalized to total MG (GFP^+^ or TdTomato^+^) or retinal length, it would be useful to clarify whether near-complete transduction is assumed, or if additional information on transduction efficiency can be provided.

(3) In Figure S10, the reduced MG proliferation observed in the CCA + Rbpj deletion group could also potentially reflect decreased GFAP promoter activity in dedifferentiated MG following Rbpj deletion. Alternatively, MG-derived cells may be more fragile under these conditions.

(4) In the CCA + Rbpj deletion condition, do MG undergo single or multiple rounds of cell division?

(5) What fraction of neuron-like cells (bipolar- and amacrine-like) arises from proliferation versus direct transdifferentiation? Quantification of MG-derived cells expressing neuronal markers (e.g., Otx2, HuC/D), with and without EdU labeling, would help distinguish these mechanisms.

(6) In Figure S18a, the authors state that "while the neuron-like clusters were best classified as BC-like and AC-like based on their distinct marker gene expression, they also exhibited mixed expression of genes associated with other retinal neuronal types, including RGC markers (e.g., Tubb3, Myt1l, Grin1) and photoreceptor markers (e.g., Crx, Prom1, Epha10, Gucy2e, Scg3) (Fig. S18a), suggesting that the regenerated cells exist in a hybrid state" and

"MG derived neuron like cells also expressed genes characteristic of RGCs and photoreceptors, indicating enhanced lineage". However, many of these genes are not specific to RGCs or photoreceptors and are instead broadly expressed in retinal neurons or enriched in bipolar/amacrine populations. Therefore, it is unclear whether these cells exhibit hybrid RGC or photoreceptor identity.

(7) The authors provide a thorough molecular characterization of MG-derived cells through immunostaining and single-cell sequencing. However, their morphological features, synaptic connectivity (e.g., synaptic marker expression), and electrophysiological properties remain largely uncharacterized. While these experiments may be technically challenging, this limitation should be discussed.

(8) The conclusion that CCA + Rbpj deletion induces neurogenesis without compromising MG supportive functions or retinal homeostasis appears somewhat oversold. This claim is primarily based on gross retinal morphology and ZO-1 staining. Given the extent of MG dedifferentiation and ectopic cell generation in the ONL and INL, it is likely that retinal function is affected. Functional assessments (e.g., ERG) would be required to support this conclusion. The authors should consider tempering this statement.

(9) Regarding the mechanism by which CCA-induced proliferation enhances MG reprogramming in the Rbpj knockout background, one plausible explanation is that chromatin states (e.g., histone modifications and DNA methylation) are transiently reset during DNA replication and cell division. While this alone may be insufficient to activate neurogenic programs, it could synergize with Rbpj deletion to allow neurogenic transcription factors (such as Ascl1, Otx2, NeuroD1, and NeuroD2) to access previously inaccessible chromatin regions, thereby promoting MG reprogramming.

https://doi.org/10.7554/eLife.111251.1.sa1

Reviewer #2 (Public review):

Summary:

The inability of the mammalian retina to regenerate poses a major clinical challenge. Much has been learned about the regenerative potential of the retina from teleost fish, where Müller glia (MG) are able to proliferate and produce new neurons after injury. However, MG do not retain this potential in the mammalian retina. The authors showed previously that forcing MG to re-enter the cell cycle by downregulating p27 and upregulating cyclin D1 could induce MG to dedifferentiate, but the results were transient, and these cells eventually reverted back to MG and did not form neurons. Here, they expand on this to show that in MG, coupling forced cell cycle re-entry with deletion of Rbpj, which inhibits the transcriptional effects of Notch signaling, induces some MG to proliferate and take on features of multiple cell types, including MG precursor cells, amacrine-like cells, and bipolar-like cells. This work lends valuable insight into the regenerative potential of mammalian MG, particularly when Notch signaling is manipulated.

Strengths:

The major claims of the authors are well-supported. They show convincingly - and through multiple methods including immunostaining, single-nucleus RNA sequencing, and in situ hybridization - that coupling notch inhibition with cell cycle reactivation induces the expression of neuronal markers in mammalian MG. The snRNA-seq data are particularly valuable in demonstrating the induction of bipolar-cell subtypes. Edu labeling is effective in demonstrating the induction of proliferation, and the long-term viability of the generated neuron-like cells is intriguing.

Weaknesses:

Whether the newly generated neurons are functionally integrated remains unclear, and the effect of the manipulation on the function of the retina was not tested. Imaging data suggests that many of the newly generated neurons persist for months, but often appear mislocalized. It is also not clear if the manipulation of MG affects long-term MG function. Cell death was not evaluated, and although the authors evaluated the long-term effect on tight junctions, this data was not quantified, and further analysis on morphology or function was not done. Control eyes were untreated, not vehicle-injected.

https://doi.org/10.7554/eLife.111251.1.sa0